

Supporting Information

A Flexible Designing Strategy to Construct Activatable NIR-II Fluorescent Probes with Emission Maximum over 1200 nm

Kun Dou ^{†§}, Wenqi Feng^{†§}, Chen Fan[†], Yu Cao[‡], Yunhui Xiang[†], and Zhihong Liu^{*†‡}

[†] Key Laboratory of Analytical Chemistry for Biology and Medicine (Ministry of Education), College of Chemistry and Molecular Sciences, Wuhan University, Wuhan, Hubei 430072, China.

[‡] Ministry of Education Key Laboratory for the Synthesis and Application of Organic Functional Molecules and College of Chemistry and Chemical Engineering, Hubei University, Wuhan 430062, China.

*Corresponding author. E-mail: zhliu@whu.edu.cn

Table of Contents

1.	Materials and apparatus	S4
2.	Synthesis and Characterization	S4
3.	Spectroscopic measurements and solution preparation.....	S8
4.	Measurement of fluorescence quantum yield (Φ).	S9
5.	Kinetic studies	S9
6.	Photostability and specificity of probe to H_2S	S9
7.	Determine of detection limits	S10
8.	MTT assays.....	S10
9.	Biosafety of probe WH-3	S10
10.	Cell culture and fluorescence cell imaging.....	S10
11.	Scheme S1. Synthesis of probe WH-X.....	S11
12.	Table S1. Reported activatable molecular fluorescent probes for NIR-II imaging S12	
13.	Figure S1. Spectroscopic response of WH-1 to H_2S	S13
14.	Figure S2. Spectroscopic response of WH-2 to H_2S	S14
15.	Figure S3. Spectroscopic response of WH-3 to H_2S	S15
16.	Figure S4. Spectroscopic response of WH-4 to H_2S	S16
17.	Figure S5. Reaction-time profiles of WH-3 in the presence of NaHS	S17
18.	Figure S6. <i>Pseudo</i> -first-order kinetic plot of the reaction of WH-3 with NaHS	S17
19.	Figure S7. Activated ratio comparison of WH-1 and WH-3 in response to H_2S . S18	
20.	Figure S8. NIR-II fluorescence image of WH-3 in response to H_2S in PBS buffer with various long-pass filters.	S18
21.	Figure S9. Time dependent fluorescence changes of WH-3 in different mediums. S19	
22.	Table S2. Photophysical properties of probe WH-X.....	S20
23.	Figure S10. Investigation of the Specificity response of WH-3 to H_2S	S21
24.	Figure S11. Frontier orbitals of WH-X (WH-1, WH-2, WH-3, WH-4) obtained by DFT calculations.	S22
25.	Figure S12. High-resolution mass spectrometry confirmed reaction mechanism. S23	
26.	Figure S13. Cytotoxicity of the WH-3.	S23
27.	Figure S14. H&E staining results of major organs.	S24
28.	Figure S15. In vivo imaging of H_2S in tumor-bearing mice.....	S24
29.	Figure S16. The advantage of long excitation and emission wavelength in penetration.....	S26
30.	Figure S17. Time-dependent NIR-II imaging of endogenous H_2S changes by exogenous drug stimulation.....	S27
31.	Figure S18. 1H NMR of compound 1	S28
32.	Figure S19. 1H NMR of compound 2-1.....	S28
33.	Figure S20. 1H NMR of compound 2-2(1)	S29
34.	Figure S21. 1H NMR of compound 2-2(2)	S29

35.	Figure S22. ^1H NMR of compound 3-1	S30
36.	Figure S23. ^1H NMR of compound 3-2.....	S30
37.	Figure S24. ^1H NMR and ^{13}C NMR of compound 3-3	S31
38.	Figure S25. ^1H NMR of compound 3-4.....	S32
39.	Figure S26. ^1H NMR and HRMS of probe WH-1	S32
40.	Figure S27. ^1H NMR and HRMS of probe WH-2	S33
41.	Figure S28. ^1H NMR and HRMS of probe WH-3	S34
42.	Figure S29. ^1H NMR and HRMS of probe WH-4	S35
43.	References	S37

1. Materials and apparatus

In our experiments, unless otherwise stated, all reagents and materials were purchased from commercial company and used without further purification. Aminooxy acetic acid (AOAA), IR-1061 were obtained from Sigma-Aldrich. S-adenosyl-L-methionine (SAM), ICG, 3-(4,5-dimethylthiazol-2-yl)-2,5-diphenyltetrazolium bromide, 3-ethyl-2,4-dimethylpyrrole, 4-nitrothiophenol were purchased from Aladdin Reagent, Ltd. (Shanghai, China). Other reagents, including common solvents, were analytical grade or higher grade, and were used without further purification. All aqueous solutions were prepared using ultrapure water (Mill-Q, Millipore, 18.2 MΩ·cm resistivity). Mass spectrometry was performed on Ultimate3000&Compact (Bruker, Germany), Scientific LTQ Orbitrap Elite (Thermo Fisher, America) mass spectrometers. The ¹H-NMR and ¹³C-NMR spectra were acquired over a Bruker Advance III HD 400 spectrometer. Absorption spectra were recorded on a UV-vis-NIR spectrophotometer (Shimadzu UV-2550, UV-3600, Japan). NIR-II fluorescence spectra were excited by 808/980nm laser (Beijing Hi-Tech Optoelectronic Co., Ltd.) and recorded with a fluorometer (Fluorolog-3, Horiba Jobin Yvon, France). Confocal microscopy images of HCT-116 cells were conducted on Zeiss LSM 880 Microscope. *In vivo* NIR-II fluorescence images were acquired by In-Vivo Master NIR-II fluorescence imaging system (Grand Imaging Technology Co. Ltd., Wuhan).

2. Synthesis and Characterization

Synthesis of compound 1

1,1,2-Trimethyl-1H-benz[e]indole (656 mg, 3.1mmol) in 3 mL 1,2-dichlorobenzene was stirred at room temperature for 30 min and then treated with 1,3-propane sultone (422 mg, 3.5 mmol). Then, the mixture was heated to 120 °C for 18 h. After cooled and treated with ether (35 mL), product 1 was filtered out (906 mg, 91%). ¹H NMR (400 MHz, DMSO) δ 8.36 (d, *J* = 8.3 Hz, 1H), 8.29 (d, *J* = 8.9 Hz, 1H), 8.26 – 8.19 (m, 2H), 7.78 (dd, *J* = 8.4, 6.9, 1.4 Hz, 1H), 7.75 – 7.69 (m, 1H), 4.83 – 4.72 (m, 2H), 2.94 (s, 3H), 2.67 (t, *J* = 6.5 Hz, 2H), 2.22 (dt, *J* = 14.4, 7.4 Hz, 2H), 1.76 (s, 6H).

Synthesis of compound 2-1

A solution of 1,8-naphtholactam (0.85 g, 5 mmol) and potassium hydroxide (0.56 g, 10 mmol) in N-methyl-2-pyrrolidone (10 mL) was stirred at room temperature for 30 min and then treated with 1,3-propane sultone (0.66 g, 5.5 mmol). Then, the mixture was heated at 90°C for 10 h, then

cooled and treated with acetone (35 mL) to cause the crystallization of product 2-1 (1.4 g, 92%).

^1H NMR (400 MHz, DMSO) δ 8.19 (d, J = 8.1 Hz, 1H), 8.05 (d, J = 7.0 Hz, 1H), 7.87 – 7.74 (m, 1H), 7.65 (d, J = 8.4 Hz, 1H), 7.61 – 7.53 (m, 1H), 7.27 (d, J = 7.0 Hz, 1H), 3.99 (t, J = 7.0 Hz, 2H), 3.42 (d, J = 6.3 Hz, 2H), 1.99 (dt, J = 14.3, 7.2 Hz, 2H).

Synthesis of compound 2-2 (1)

Compound 2-1 (0.658 mg, 2mmol) was dissolved in 5 mL acetic acid and tetrabutylammonium bromide (708 mg, 2.2 mmol) was added into the mixture. The reaction was stirred at 90 °C for 0.5 h, and then treated with ethyl acetate dropwise. The precipitate (potassium bromide) was then filtered out after cooling. The filtrate was concentrated on a rotary evaporator and dried to obtain yellow solid (1.02 g 83%). ^1H NMR (400 MHz, DMSO) δ 8.19 (d, J = 8.1 Hz, 1H), 8.05 (d, J = 6.9 Hz, 1H), 7.84 – 7.75 (m, 1H), 7.64 (d, J = 8.3 Hz, 1H), 7.61 – 7.53 (m, 1H), 7.27 (d, J = 6.9 Hz, 1H), 3.99 (t, J = 7.0 Hz, 2H), 3.19 – 3.13 (m, 8H), 2.46 (dd, J = 8.5, 6.6 Hz, 2H), 2.07 – 1.91 (m, 2H), 1.61 – 1.52 (m, 8H), 1.31 (dd, J = 14.7, 7.3 Hz, 8H), 0.93 (t, J = 7.3 Hz, 12H).

Synthesis of compound 2-2 (2)

Under nitrogen atmosphere, 2 mL methyl magnesium chloride (3.0 M solution in tetrahydrofuran) was added dropwise to a stirred solution of solid 2-2 (1) (0.8 g, 1.33 mmol) in anhydrous tetrahydrofuran over 50 min at 55 °C. Then, the mixture was stirred at 55°C for another 1 h, cooled to R.T and neutralized by dropwise addition of 1M hydrochloric acid. The obtained solution was consecutively diluted with ethanol (30 mL) and ether (30 mL) and cooled to -20 °C for several hours, resulted in crystallization of product 2-2 (2) (0.34 g, 64 %). ^1H NMR (400 MHz, D₂O) δ 8.46 (d, J = 7.2 Hz, 1H), 8.37 (d, J = 8.0 Hz, 1H), 8.04 (dd, J = 10.6, 8.1 Hz, 2H), 7.82 (t, J = 7.6 Hz, 1H), 7.68 (t, J = 7.8 Hz, 1H), 4.67 (s, 3H), 4.59 (t, J = 7.6 Hz, 2H), 2.96 (t, J = 7.1 Hz, 2H), 2.27 (dt, J = 14.6, 7.3 Hz, 2H).

Synthesis of compound 3-1

3 mL anhydrous DMF and 3 mL POCl₃ were added into a 25 ml round-bottom flask and stirred at 0 °C for 1 h under a nitrogen atmosphere. After warmed to room temperature, mixture was stirred for another 30 min. Compound 3-chloro-5,7-dimethyl-6-ethyl-8-phenyl-BODIPY (200 mg, 0.52 mmol, obtained from our laboratory) was dissolved in 10 ml anhydrous CH₂Cl₂ and slowly dropped into the mixture. Under room temperature the mixture was stirred for 15 h. After the reaction completed, aqueous NaHCO₃ and NaOH was added carefully, then the mixture was

extracted with DCM (20 mL \times 3). The organic layer was dried over Na₂SO₄ and concentrated under reduced pressure. The crude product was purified by silica gel chromatography (silica gel, (20:1, v/v) petroleum ether/ethyl acetate) to give **3-1** (87 mg, 39.0 %) as a brown solid. ¹H NMR (400 MHz, CDCl₃) δ 9.79 (s, 1H), 7.48 – 7.41 (m, 3H), 7.23 (dd, J = 7.9, 1.5 Hz, 2H), 6.57 (s, 1H), 2.62 (s, 3H), 2.32 (q, J = 7.6 Hz, 2H), 1.42 (s, 3H), 0.98 (t, J = 7.6 Hz, 3H).

Synthesis of compound 3-2

Compound 3-1 (77.2 mg, 0.2 mmol) and 4-dimethylaminopyridine (DMAP, 30mg, 0.25 mmol) were dissolved in anhydrous acetonitrile (25 ml) and then 4-nitrothiophenol (48 mg, 0.31 mmol) was added. The reaction was stirred at 40°C for 30 min, then solvent was removed by rotary evaporator and the crude residue was purified by column chromatography (petroleum ether/ethyl acetate = 8:1, v/v) to give the product as a red solid (75 mg, 81%). ¹H NMR (400 MHz, CDCl₃) δ 9.82 (s, 1H), 8.03 (d, J = 9.0 Hz, 2H), 7.55 – 7.44 (m, 3H), 7.29 (dd, J = 7.8, 1.6 Hz, 2H), 7.22 (d, J = 2.1 Hz, 1H), 7.20 (d, J = 2.1 Hz, 1H), 6.70 (s, 1H), 2.60 (s, 3H), 2.40 – 2.19 (m, 2H), 1.45 (s, 3H), 0.97 (t, J = 7.6 Hz, 3H).

Synthesis of compound 3-3

A solution of compound 3-2 (50 mg, 0.1 mmol), 3,4-dimethoxybenzaldehyde (50 mg, 0.3 mmol) and 100 μ L piperidine in (20 mL) anhydrous methylbenzene was heated to reflux for 1 h, then cooled to room temperature, and then excess methylbenzene was removed under vacuum. The residue was purified by silica gel chromatography (silica gel, petroleum ether/ethyl acetate = 10:1-8:1, v/v) to give pure compound 3-3 as a purple solid (13 mg, 20.3 %). ¹H NMR (400 MHz, CDCl₃) δ 9.89 (s, 1H), 8.09 (d, J = 9.0 Hz, 2H), 7.65 (d, J = 16.6 Hz, 1H), 7.55 (dd, J = 11.0, 4.8 Hz, 4H), 7.39 (dd, J = 7.5, 1.8 Hz, 2H), 7.30 (d, J = 9.0 Hz, 2H), 7.27 (d, J = 2.0 Hz, 1H), 7.10 (d, J = 1.9 Hz, 1H), 6.90 (d, J = 8.4 Hz, 1H), 6.76 (s, 1H), 3.95 (d, J = 8.3 Hz, 6H), 2.69 (q, J = 7.5 Hz, 2H), 1.55 (s, 3H), 1.21 (t, J = 7.5 Hz, 3H). ¹³C NMR (101 MHz, CDCl₃) δ 186.26, 163.00, 152.05, 149.44, 147.23, 145.82, 144.71, 144.31, 139.00, 138.24, 137.83, 137.50, 133.20, 129.91, 128.96, 128.89, 128.87, 126.90, 124.22, 123.19, 121.25, 116.51, 111.23, 110.46, 56.40, 18.74, 13.40, 12.42.

Synthesis of compound 3-4

Compound 3-2 (50 g, 0.1 mmol) and 4-dimethylaminobenzaldehyde (47 mg, 0.3 mmol) were dissolved in 20 ml anhydrous methylbenzene, and then 100 μ L piperidine was added into the

mixture. Reaction mixture was stirred at 110 °C for 1 hour. After the reaction was completed, excess methylbenzene was removed under reduced pressure, and the residue was purified by silica gel chromatography (silica gel, petroleum ether/ethyl acetate = 10:1-8:1-6:1, v/v) to give pure compound 3-4 as blue solid (11 mg 18.2 %) ¹H NMR (400 MHz, CDCl₃) δ 9.91 (s, 1H), 8.09 (d, *J* = 9.0 Hz, 2H), 7.62 (s, 2H), 7.57 (d, *J* = 8.9 Hz, 2H), 7.55 – 7.50 (m, 3H), 7.37 (dd, *J* = 7.1, 2.2 Hz, 2H), 7.29 (d, *J* = 9.0 Hz, 2H), 6.76 (d, *J* = 8.6 Hz, 2H), 6.69 (s, 1H), 3.09 (s, 6H), 2.69 (q, *J* = 7.5 Hz, 2H), 1.52 (s, 3H), 1.20 (t, *J* = 7.5 Hz, 3H).

Synthesis of probe **WH-1**

Compound 1 (47.5 mg, 0.15 mmol) and compound 3-2 (50 mg, 0.1 mmol) were dissolved in 20 mL anhydrous EtOH. The reaction mixture was heated to reflux for 12 h. After removal of the solvent, the crude product was purified by silica gel flash chromatography (CH₂Cl₂/MeOH = 50:1-20:1, v/v) to afford compound WH-1 (65 mg, 85%). ¹H NMR (400 MHz, CDCl₃) δ 8.18 (d, *J* = 15.2 Hz, 2H), 8.12 (d, *J* = 8.8 Hz, 2H), 8.07 (d, *J* = 8.7 Hz, 2H), 8.02 (d, *J* = 8.6 Hz, 1H), 7.93 (s, 1H), 7.81 – 7.73 (m, 3H), 7.70 (d, *J* = 7.3 Hz, 1H), 7.63 (t, *J* = 7.9 Hz, 2H), 7.52 (d, *J* = 6.8 Hz, 2H), 7.36 (d, *J* = 8.9 Hz, 2H), 4.91 (t, *J* = 12.6 Hz, 2H), 3.03 – 2.90 (m, 2H), 2.68 (s, 3H), 2.42 (dd, *J* = 15.2, 7.6 Hz, 2H), 2.36 (d, *J* = 7.4 Hz, 2H), 1.61 (s, 3H), 1.07 (t, *J* = 7.6 Hz, 3H). HRMS: calcd for C₄₄H₄₂BF₂N₄O₅S₂⁺ [M]⁺ 819.2652 found 819.2684.

Synthesis of probe **WH-2**

A mixture of compound 2-2 (2) (58 mg, 0.2 mmol) and (50 mg, 0.1 mmol) compound 3-2 in 20 mL ethanol was stirred at 90 °C for 3.5 h. After the reaction, solvent was removed under reduced pressure and the crude residue was purified by column chromatography ((silica gel, 50:1-15:1 v/v CH₂Cl₂/MeOH) to give the product as a red solid. Yield: 51mg (68 %). ¹H NMR (400 MHz, CDCl₃) δ 8.47 (d, *J* = 15.5 Hz, 1H), 8.38 (d, *J* = 8.0 Hz, 1H), 8.27 (d, *J* = 15.5 Hz, 1H), 8.15 (dd, *J* = 11.7, 8.3 Hz, 3H), 8.04 (d, *J* = 8.2 Hz, 1H), 7.88 (dd, *J* = 16.4, 7.9 Hz, 2H), 7.82 (s, 1H), 7.77 (dt, *J* = 10.9, 7.5 Hz, 4H), 7.53 (d, *J* = 6.9 Hz, 2H), 7.36 (d, *J* = 8.9 Hz, 2H), 4.96 (t, *J* = 7.4 Hz, 2H), 3.08 – 2.90 (m, 2H), 2.67 (s, 3H), 2.42 (dd, *J* = 15.2, 7.5 Hz, 4H), 1.61 (s, 3H), 1.07 (t, *J* = 7.6 Hz, 3H). HRMS: calcd for C₄₁H₃₆BF₂N₄O₅S₂⁺ [M]⁺ 777.2183 found 777.2205.

Synthesis of probe **WH-3**

To a solution of compound 3-3 (6.5 mg, 0.01 mmol) in 15 mL EtOH, compound 2-2 (14.5 mg,

0.05 mmol) was added and heated to 90 °C for 3 h, and then concentrated under reduced pressure. The crude product was purified by column chromatography to give a blue solid (silica gel, CH₂Cl₂/MeOH = 50:1-15:1, v/v) 4.5 mg, 50%). ¹H NMR (400 MHz, CDCl₃) δ 8.49 (d, *J* = 15.6 Hz, 1H), 8.37 (d, *J* = 8.1 Hz, 1H), 8.23 (d, *J* = 15.6 Hz, 1H), 8.14 (d, *J* = 7.3 Hz, 3H), 8.05 (d, *J* = 8.2 Hz, 1H), 7.87 (dd, *J* = 9.1, 6.0 Hz, 2H), 7.82 – 7.73 (m, 5H), 7.61 (d, *J* = 14.0 Hz, 2H), 7.56 (d, *J* = 6.7 Hz, 2H), 7.38 (d, *J* = 8.8 Hz, 2H), 7.28 (s, 1H), 7.12 (d, *J* = 1.5 Hz, 1H), 6.91 (d, *J* = 8.4 Hz, 1H), 4.94 (t, *J* = 8.2 Hz, 2H), 3.97 (d, *J* = 9.8 Hz, 6H), 3.04 – 2.95 (m, 2H), 2.72 (q, *J* = 7.7 Hz, 2H), 2.46 – 2.37 (m, 2H), 1.45 (s, 3H), 1.02 (t, *J* = 15.0 Hz, 3H). HRMS: calcd for C₅₀H₄₄BF₂N₄O₇S₂⁺ [M]⁺ 925.2707 found 925.2711.

Synthesis of probe **WH-4**

A mixture of compound 3-4 (6.3 mg, 0.01 mmol) and compound 2-2 (14.5 mg, 0.05 mmol) in 15 mL anhydrous ethanol was stirred at 90 °C for 3 h. Then, the mixture was cooled, and solvents was removed on a rotary evaporator. The crude product was purified by column chromatography to give a blue solid (silica gel, 50:1-15:1 v/v CH₂Cl₂/MeOH) 3 mg, 33.3%). ¹H NMR (400 MHz, CDCl₃) δ 8.52 (d, *J* = 15.4 Hz, 1H), 8.35 (d, *J* = 8.0 Hz, 1H), 8.15 (dd, *J* = 12.5, 8.2 Hz, 3H), 8.08 (d, *J* = 15.6 Hz, 1H), 8.02 (d, *J* = 8.2 Hz, 1H), 7.93 (d, *J* = 7.3 Hz, 1H), 7.86 (t, *J* = 7.8 Hz, 1H), 7.79 (d, *J* = 7.9 Hz, 1H), 7.73 (dd, *J* = 15.8, 7.6 Hz, 3H), 7.63 (d, *J* = 5.7 Hz, 2H), 7.58 (d, *J* = 8.6 Hz, 3H), 7.53 (d, *J* = 6.1 Hz, 2H), 7.38 (d, *J* = 8.9 Hz, 2H), 6.76 (d, *J* = 8.4 Hz, 2H), 4.94 (t, *J* = 6.8 Hz, 2H), 3.11 (s, 6H), 3.05 – 2.97 (m, 2H), 2.72 (q, *J* = 7.3 Hz, 2H), 2.46 – 2.33 (m, 2H), 1.60 (s, 3H), 1.22 (t, *J* = 7.6 Hz, 3H). HRMS: calcd for C₄₁H₃₆BF₂N₄O₅S₂⁺ [M]⁺ 908.2918 found 908.29425.

3. Spectroscopic measurements and solution preparation.

Probes, including **WH-1**, **WH-2**, **WH-3** and **WH-4** were dissolved in DMSO to prepare the stock solution with a concentration of 1mM. Unless otherwise noted, all the absorption/fluorescence titration were tested in PBS buffer (PBS/CH₃CN, 7:3, v/v, 20 mM, pH 7.4, 37 °C). Absorption spectra were obtained with 1.0-cm quartz cells. Fluorescence emission spectra at NIR-I region was obtained with a Xenon lamp and NIR-II spectra was obtained by 808/980 nm laser. For absorption/fluorescence spectra measurements, 10 μM probe and various amounts of NaHS solution were added into CH₃CN/PBS buffer. After incubated at 37 °C for 30 min, spectrum scan was then conducted.

4. Measurement of fluorescence quantum yield (Φ).

The quantum yields were calculated by the equation: $\Phi_{\text{sam}} = \Phi_{\text{ref}} \times (K_{\text{sam}}/K_{\text{ref}}) \times (n_{\text{sam}} / n_{\text{ref}})^2$, where subscripts sam and ref denote test sample and reference, respectively. Φ is the fluorescence quantum yield, n is the refractive index of the solvent and K is the slope of the plot, where the slope was determined by plotting the integrated fluorescence intensity vs absorbance value. In brief, five samples with different absorbance at 808/980 nm were prepared, and then collected the fluorescence integrated intensity under corresponding excitation wavelength. Notably, in order to maximize illumination homogeneity and optical transparency, all absorbance in tests were kept below 0.1 at excitation wavelength. In this work, the quantum yields of **WH-X-HS** in PBS buffer was determined with the reference of IR 1061 ($\Phi = 1.7\%$ in CH_2Cl_2).¹

5. Kinetic studies

The rate constant was determined from the fluorescence titration data based on a reported method⁹. The reaction of the probe **WH-3** (10 μM) with NaHS in PBS/ CH_3CN (7:3, v/v, 20 mM, 37 °C) was monitored using the fluorescence intensity at 1145 nm. The *pseudo*-first-order rate constant of the reaction was determined by fitting the fluorescence intensities of the samples to the *pseudo*-first-order equation:

$\ln [(F_{\text{max}} - F_t) / F_{\text{max}}] = -k't$. Where F_t and F_{max} are the fluorescence intensities at 1140 nm at time t and the maximum value obtained after the reaction complete. k' is the *pseudo*-first order rate constant. The *pseudo*-first-order plots of the reaction (**WH-3** with 10 equiv. NaHS) is shown in Figure S15.

6. Photostability and specificity of probe to H_2S

Firstly, the photostability of **WH-3** and **WH-3-HS** were investigated, using the commercially available dye ICG as a reference. Probes and ICG were dissolved in the mixture solution of PBS/ CH_3CN (V/V = 7:3), and the final concentration was 10.0 μM . Under 808/980 nm laser with a power density of 0.2 W/cm^2 , the change of fluorescence intensity was recorded for 30 min. The emission intensity of **WH-3**, **WH-3-HS** and ICG was measured every 2.5 min.

Then, to examine the selectivity of **WH-3** to H_2S , several biological species, including reactive oxygen species (H_2O_2 , HClO) reactive sulfur species (Cys, Hcy, GSH, SO_2 , Na_2S_4), reactive nitrogen species (ONOO^- , NO) and metal ions were respectively added into the mixture solution of PBS/ CH_3CN (V/V = 7:3) with **WH-3** (10 μM). After incubation at 37 °C for 30 min,

fluorescence spectra were detected. Finally, we measured the optical profile of **WH-3** (10 μ M) upon treating with H₂S (100 μ M) in different pH conditions (4.03-8.57) to further assess the stability of probe to biological environments. All the solutions were excited at 980 nm and emission spectra were collected at 1020-1400 nm.

7. Determine of detection limits

Detection limit of H₂S was calculated by the formula: detection limit = 3 SD/ k, where k is the slope of the fluorescence titration curve equation and SD represents the standard deviation for 11 blank samples.

8. MTT assays

MTT assay was performed to evaluate the cytotoxicity of probe. HCT-116 cells were plated in 96-well plates and incubated for 24 h to adhere. Then, various concentrations of probe (0, 5, 10, 15, 20, 25, 30, 50 μ M) that diluted by fresh DMEM medium were added into cells, and then co-incubated for another 24 h. Next, 10 μ L of methylthiazolyl tetrazolium (MTT) (5 mg/mL) was added to each well and further incubated at 37°C for 4 hours in 5% CO₂. Before evaluation, 100 μ L of DMSO was added to dissolve formazan. The absorbance was measured at 570 nm with microplate reader (Thermo Fisher Scientific, USA). The cell viability was calculated as (%) = (OD₅₇₀ (Experiments) – OD₅₇₀ (Blank)) / (OD₅₇₀ (Control) – OD₅₇₀ (Blank)). All experiments were performed in 9 replicates. The cell viability was expressed by the average values \pm standard deviation (SD).

9. Biosafety of probe WH-3

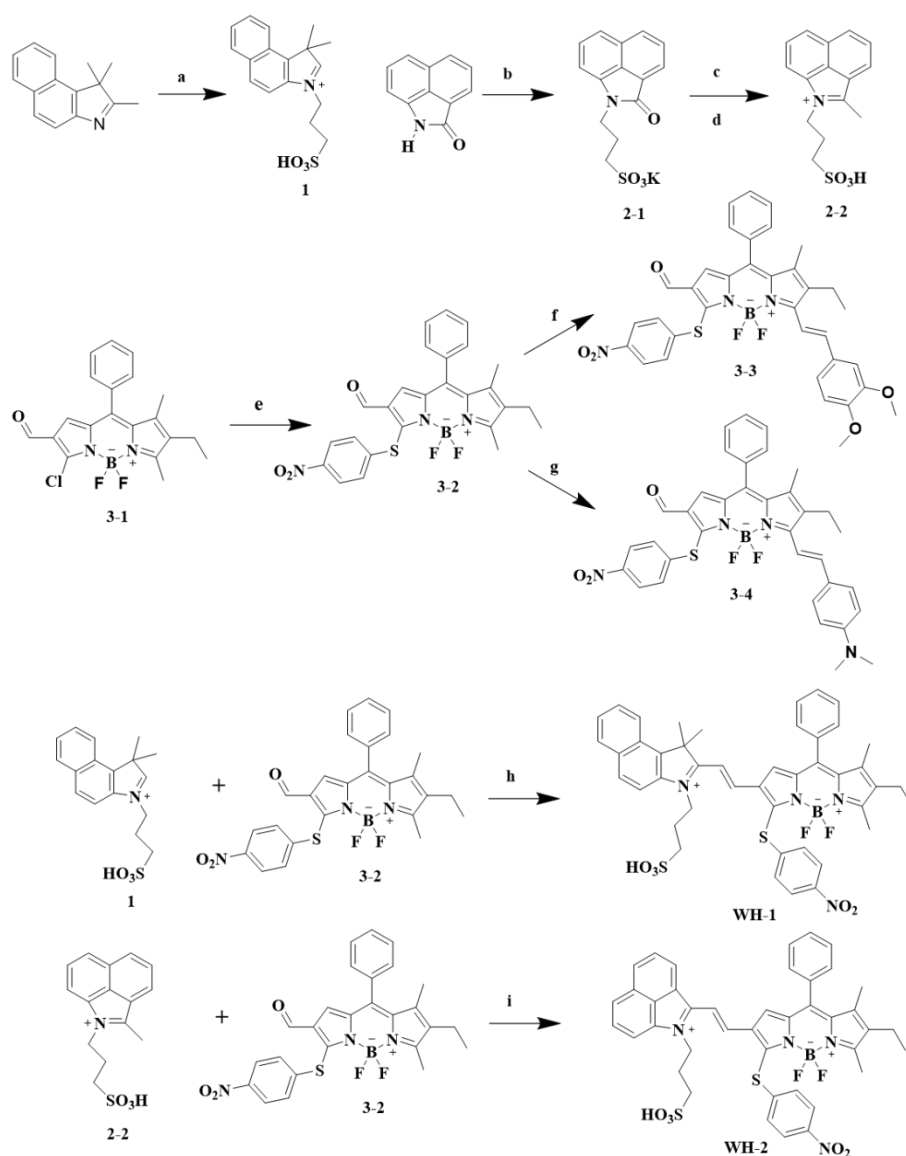
WH-3 (1mmol, 100 μ L) was intravenously (i.v.) injected into health female Balb/c mice with a body weight of about 20 g. 12h after probe injection, the major organs (heart, spleen, liver, lung and kidney) were obtained for H&E staining.

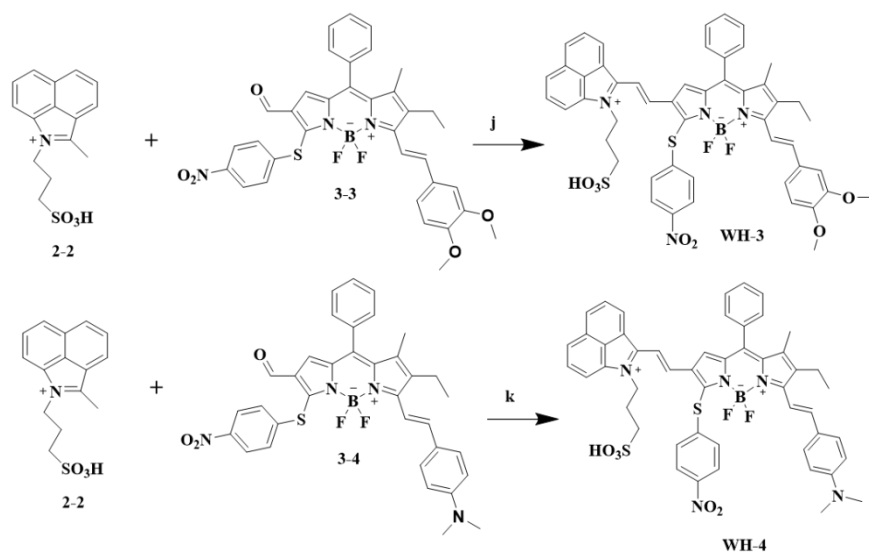
10. Cell culture and fluorescence cell imaging

In this work, HCT-116 cells were obtained from the Committee on Type Culture Collection of Chinese Academy of Sciences (Shanghai, China), which were incubated in DMEM (Dulbecco's Modified Eagle Medium) supplemented with 10% fetal bovine serum (FBS) and 1% penicillin-streptomycin (100 U/mL, 100 μ g/mL, Invitrogen) at 37 °C under a humidified atmosphere containing 5% CO₂. Before imaging, cells were placed at 25-Petri dishes and allowed to adhere for 24 hours. To verify **WH-3** could be applied for monitoring H₂S fluctuation in cells,

confocal imaging at NIR-I window was firstly performed. Control group: cells only incubated with **WH-3** (10 μ M) for 60 min. Experimental groups: group 1, **WH-3** (10 μ M) and 40 μ M NaHS were co-incubated cells for 60 min. Group 2, aminooxy acetic acid (AOAA, 25 μ M), a common used CBS inhibitor, was firstly added into the cells for 4h, and then cells were treated with **WH-3** (10 μ M) for 60 min. Fluorescence imaging was performed on a Zeiss LSM 880 Microscope with a $\times 20$ objective lens. Confocal imaging parameters: red channel (λ_{ex} = 594 nm, λ_{em} = 650-750 nm). Finally, above cells were collected in centrifuge tube for NIR-II fluorescence imaging. Cells imaging was collected at 1100-1700 nm under 980 nm laser excitation (80 mW/cm², exposure time: 300 ms, 1100 nm LP.).

11. Scheme S1. Synthesis of probe WH-X





a: 1,3-propane sultone / 1,2-dichlorobenzene b: 1,3-propane sultone / N-methyl-2-pyrrolidone c: tetrabutylammonium bromide / acetic acid d: CH_3MgBr /THF e: 4-Nitrothiophenol / CH_3CN_3 f: 3,4-dimethoxybenzaldehyde/pyridine/methylbenzene g: 4-dimethylaminobenzaldehyde/pyridine/methylbenzene h: j: i: k EtOH

12. Table S1. Reported activatable molecular fluorescent probes for NIR-II imaging

probe	Absorption (nm)	Emission (nm)	targets
BOD-M- β -Gal ²	723	853	β -Galactosidase
NTR-InD ³	730	900	nitro reductase
NIR-II-RT-ADP ⁴	854	918	adenosine triphosphate
NP-Q-NO ₂ ⁵	664/808	780/922	nitro reductase
IRBTP-B ⁶	785	970	peroxynitrite (ONOO ⁻)
IR-1041-MZ ⁷	980	1046	nitro reductase
Hydro-1080 ⁸	1021	1044	Hydroxyl radical ($\cdot\text{OH}$)
WH-1	762	925	H ₂ S
WH-2	850	1060	H ₂ S
WH-3	925	1140	H ₂ S
WH-4	960	1205	H ₂ S

13. Figure S1. Spectroscopic response of WH-1 to H₂S.

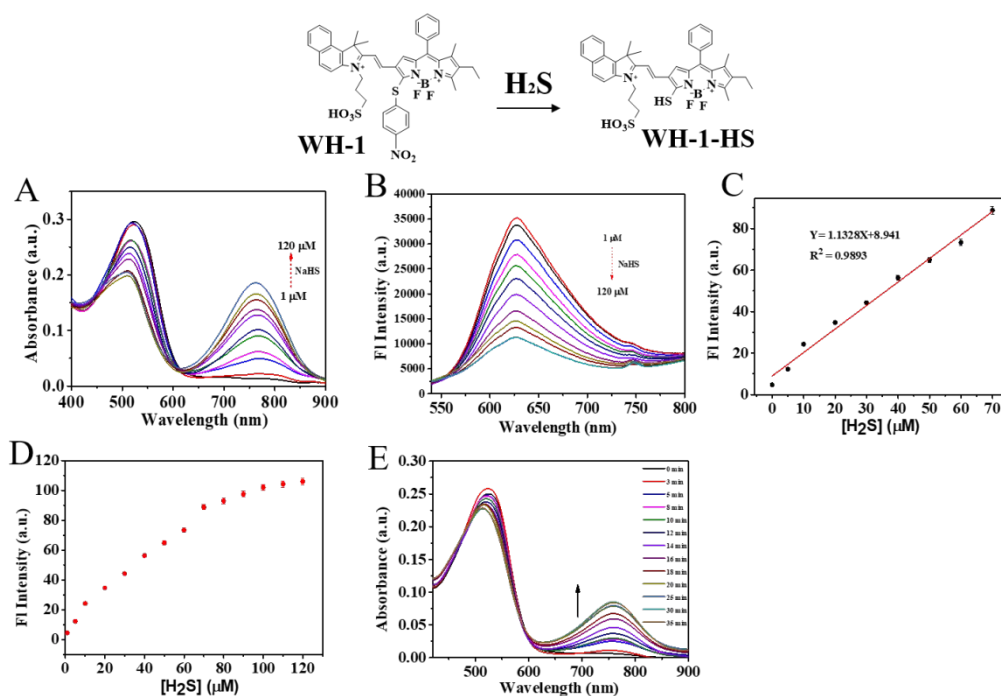


Figure S1. Spectroscopic response of WH-1 to H₂S. (A) Vis-NIR absorption spectra of WH-1 in response to 1-120 μM NaHS. (B) NIR-I fluorescence spectra of WH-1 in response to 1-120 μM NaHS (Xenon lamp, 510 nm excitation) (C) Linear relationship between fluorescence intensity at 925 nm and [NaHS] in the range of 1-70 μM. (D) Titration curve of WH-1 to NaHS. (E) Response time of WH-1 to NaHS. Detection was performed in mixed solvent (PBS/CH₃CN, 7:3, v/v, 20 mM, pH 7.4, 37 °C). NIR-I fluorescence spectra were collected under 520 nm excitation.

14. Figure S2. Spectroscopic response of WH-2 to H₂S.

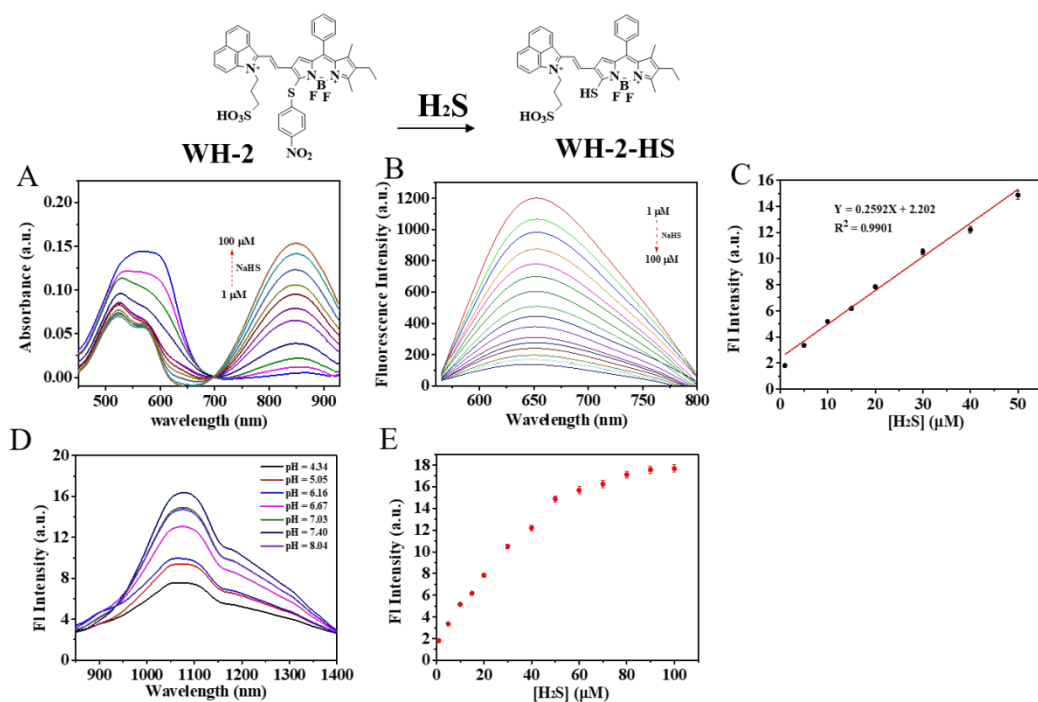


Figure S2. Spectroscopic response of WH-2 to H₂S. (A) Vis-NIR absorption spectra of **WH-2** in response to 1-100 μ M NaHS. (B) NIR-I fluorescence spectra of **WH-2** in response to 1-100 μ M NaHS (Xenon lamp, excitation: 560 nm). (C) Linear relationship between fluorescence intensity at 1060 nm and [NaHS] in the range of 1-50 μ M. (D) pH stability of **WH-2** in the range of 4.34–8.04. (E) Titration curve of **WH-2** to NaHS. Detection was performed in mixed solvent (PBS/CH₃CN, 7:3, v/v, 20 mM, pH 7.4, 37 °C). NIR-II Fluorescence was collected under 808 nm laser excitation.

15. Figure S3. Spectroscopic response of WH-3 to H₂S.

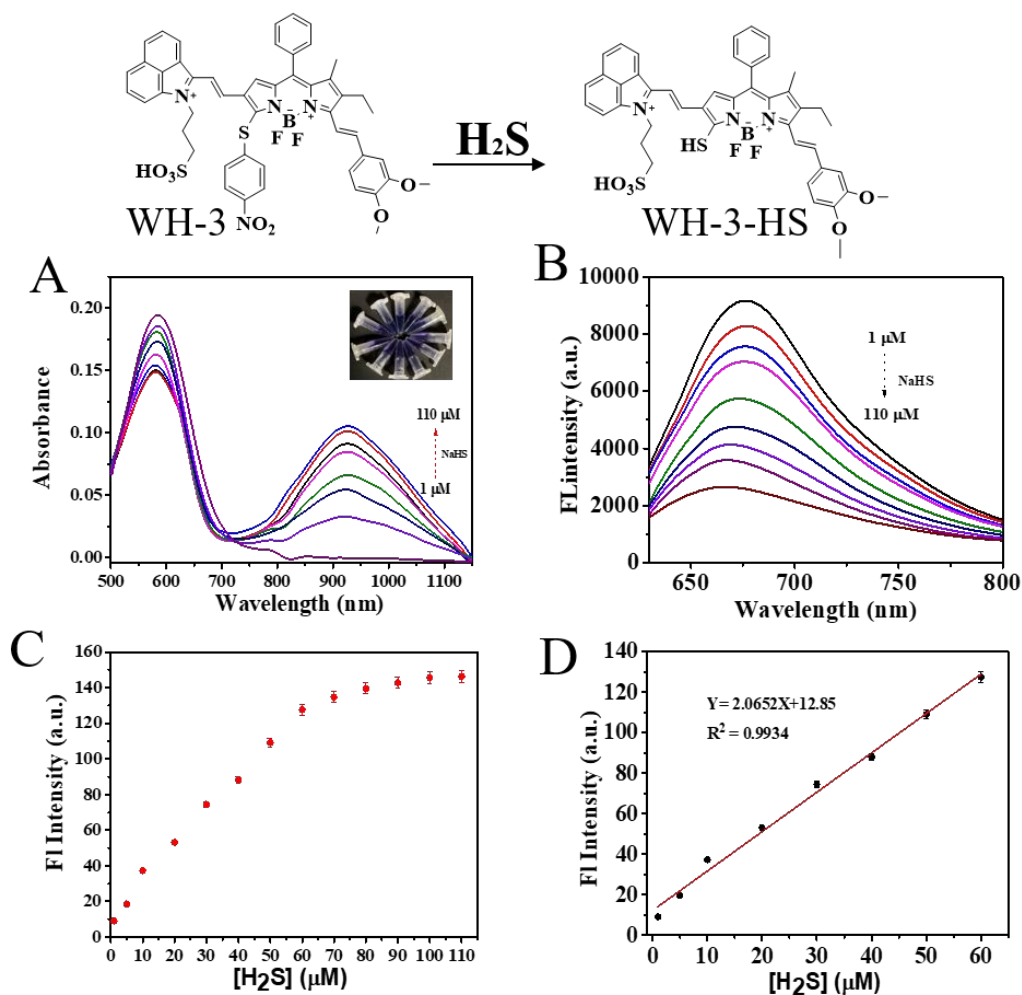


Figure S3. Spectroscopic response of WH-3 to H₂S. (A) Vis-NIR absorption spectra of **WH-3** in response to 1-110 μ M NaHS. (B) NIR-I fluorescence spectra of **WH-3** in response to 1-110 μ M NaHS (Xenon lamp, 575 nm excitation). (C) Titration curve of **WH-3** to NaHS. (D) Linear relationship between fluorescence intensity at 1140 nm and [NaHS] in the range of 1-60 μ M. Detection was performed in mixed solvent (PBS/CH₃CN, 7:3, v/v, 20 mM, pH 7.4, 37 $^{\circ}$ C). NIR-II fluorescence was collected under 980 nm laser excitation.

16. Figure S4. Spectroscopic response of WH-4 to H₂S.

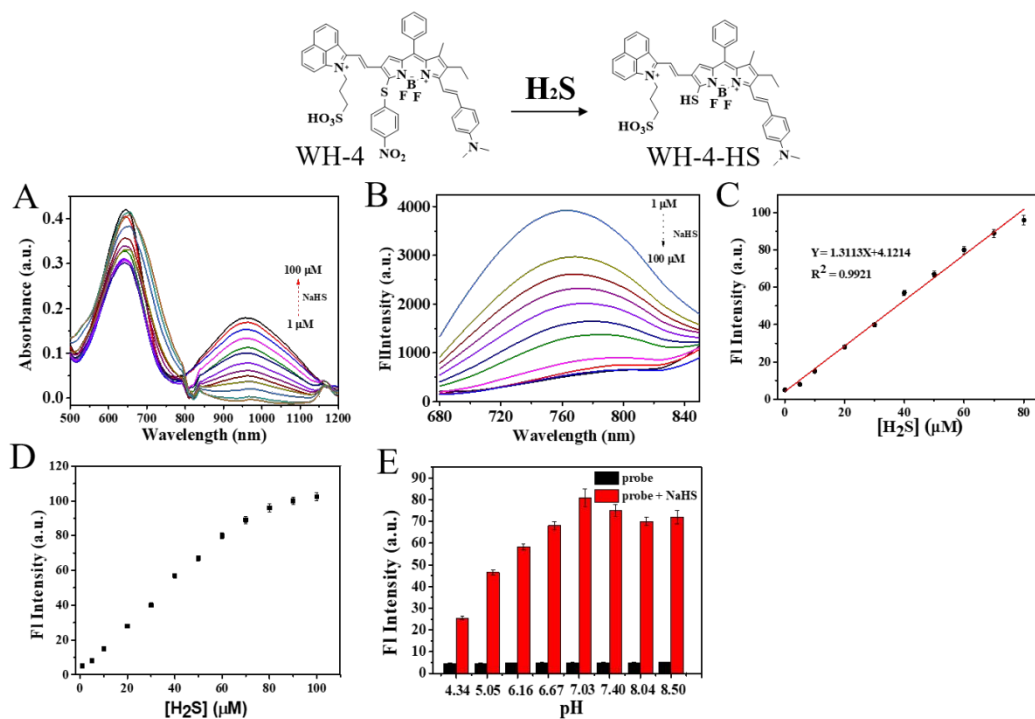


Figure S4. Spectroscopic response of WH-4 to H₂S. (A) Vis-NIR absorption spectra of **WH-4** in response to 1-100 μ M NaHS. (B) NIR-I fluorescence spectra of **WH-4** in response to 1-100 μ M NaHS (Xenon lamp, 645 nm excitation). (C) Linear relationship between fluorescence intensity at 1205 nm and [NaHS] in the range of 1-80 μ M. (D) Titration curve of **WH-4** to NaHS. (E) pH stability of WH-4 to NaHS (50 μ M) in the range of 4.34–8.04. Detection was performed in mixed solvent (PBS/CH₃CN, 7:3, v/v, 20 mM, pH 7.4, 37 $^{\circ}$ C). NIR-II fluorescence was collected under 980 nm laser excitation.

17. Figure S5. Reaction-time profiles of WH-3 in the presence of NaHS

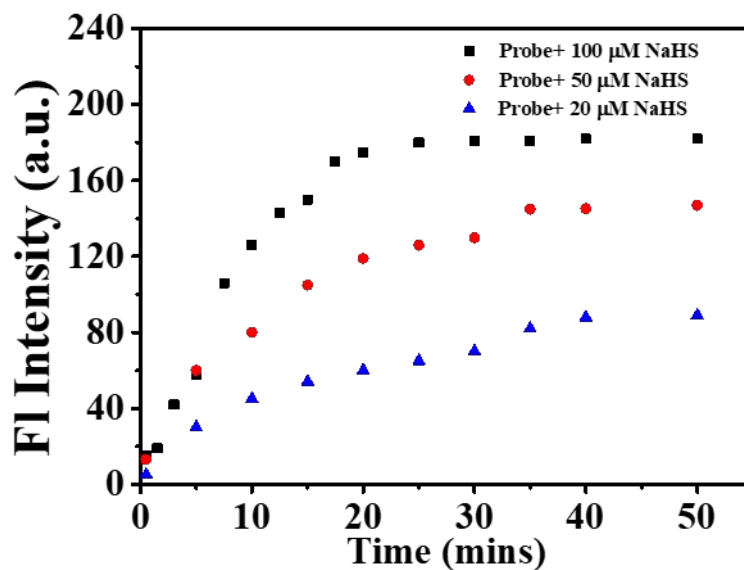


Figure S5. Reaction-time profiles of **WH-3** (10 μM) in the presence of NaHS (20 μM , 50 μM and 100 μM). The fluorescence intensities at 1140 nm were monitored at several timepoints in PBS buffer (PBS/ CH_3CN , 7:3, v/v, 20 mM, 37 $^\circ\text{C}$, 980 Ex).

18. Figure S6. *Pseudo*-first-order kinetic plot of the reaction of WH-3 with NaHS

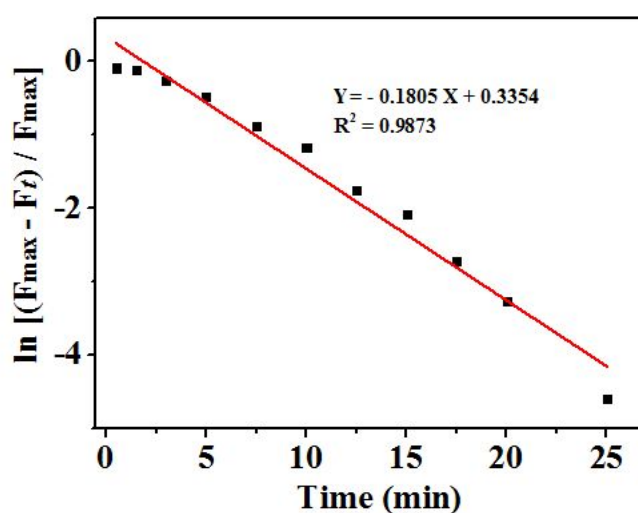


Figure S6. *Pseudo*-first-order kinetic plot of the reaction of **WH-3** (10 μM) with NaHS (10 equiv.) in PBS/ CH_3CN (7:3, v/v, 20 mM, 37 $^\circ\text{C}$). The negative slope of the line provides the *pseudo*-first-order rate constant for H_2S : $k = 0.1805 \text{ min}^{-1}$

19. Figure S7. Activated ratio comparison of WH-1 and WH-3 in response to H_2S .

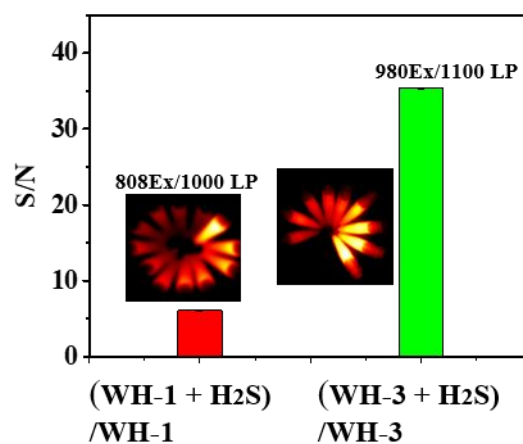


Figure S7. Activated ratio comparison of WH-1 and WH-3 in response to H_2S . Activated ratio comparison of **WH-1** (10 μM) and **WH-3** (10 μM) in response to 1-110 μM NaHS under 808/980 excitation with 1000/1100 long-pass filter. Activated ratio values were calculated by dividing average signal intensity of WH-X-HS by the average signal intensity of **WH-X**.

20. Figure S8. NIR-II fluorescence image of WH-3 in response to H_2S in PBS buffer with various long-pass filters.

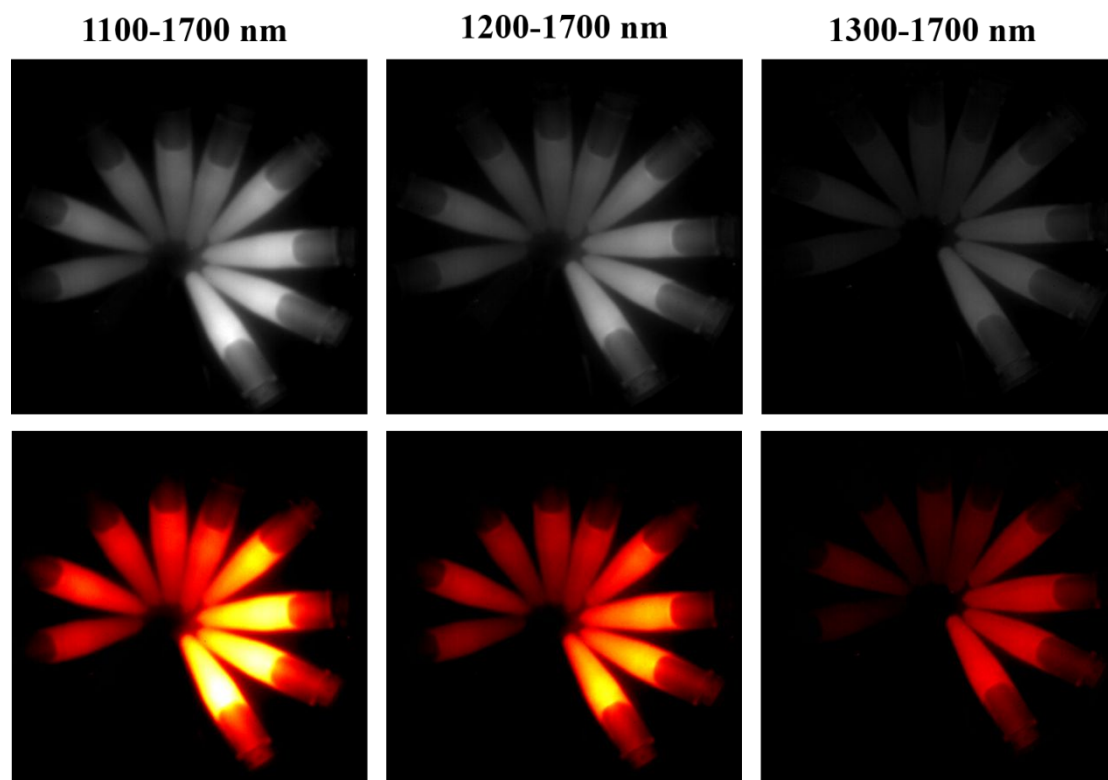


Figure S8. NIR-II fluorescence image of WH-3 in response to H₂S in PBS buffer with various long-pass filters. NIR-II fluorescence image of WH-3 in response to 1-110 μ M NaHS in PBS buffer (PBS/CH₃CN, 7:3, v/v, 20 mM, pH 7.4, 37 $^{\circ}$ C) with various long-pass filters (from left to right :1100, 1200 and 1300 nm long-pass filters) under 980 nm excitation (50 mW/cm²), exposure time: 200 ms.

21. Figure S9. Time dependent fluorescence changes of WH-3 in different mediums.

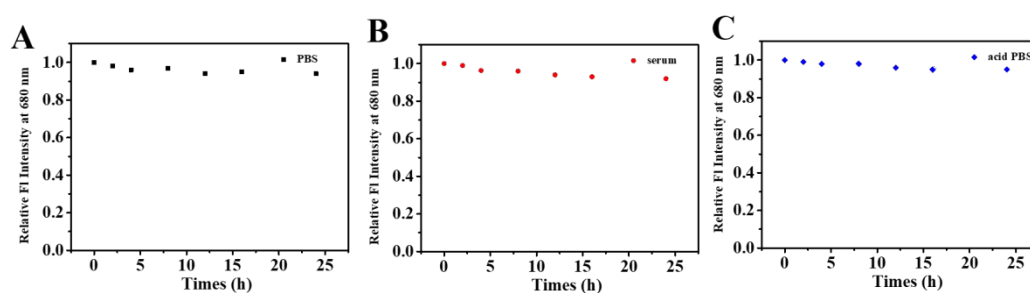
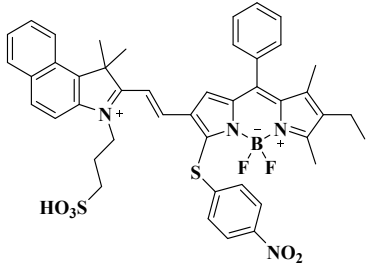
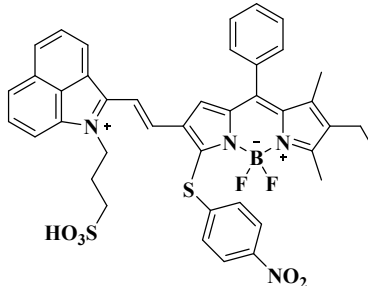
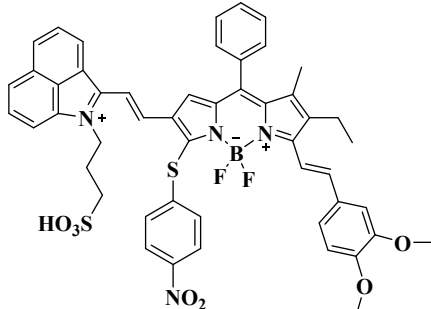
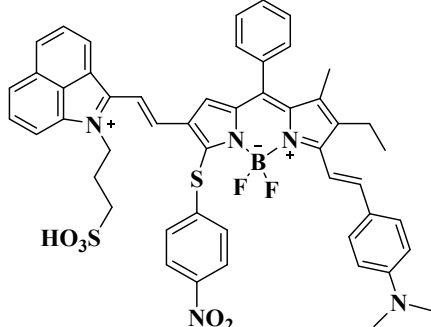


Figure S9. Time dependent fluorescence changes of WH-3 in (A) PBS buffer, (B) serum and (C) acid PBS (pH = 6.2).

22. Table S2. Photophysical properties of probe WH-X

probe	Absorption (nm)	Emission (nm)	Detection of limit (nM)	Stokes shift	Quantum yield (%)
	762	925	72	163	0.206
	850	1060	215	210	0.05
	925	1140	51	215	0.17
	960	1205	83	245	0.05

23. Figure S10. Investigation of the Specificity response of WH-3 to H₂S.

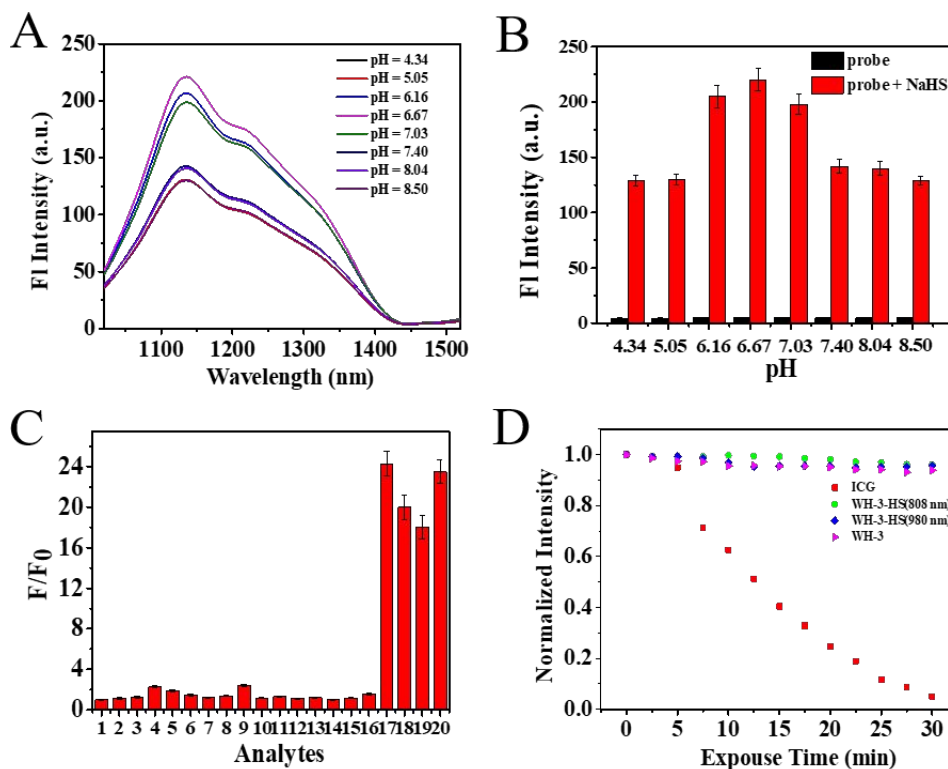


Figure S10. Investigation of the Specificity response of WH-3 to H₂S. (A)&(B) The effect of pH values (pH ranges from 4.34 to 8.50) on the fluorescence intensity at 1140 nm of **WH-3** (10 μ M) in the presence of NaHS (100 μ M)). Fluorescence intensity was measured at 1140 nm under 980 nm laser excitation. (C) Response of 10 μ M **WH-3** to various interfering species and NaHS. Interfering species were incubated with the probe in mixed solvent (PBS/CH₃CN, 7:3, v/v, 20 mM, pH 7.4) for 40 min. Fluorescence intensity ratio F/F_0 (F_0 represents the fluorescence intensity of WH-3 itself) was measured at 1140 nm under 980 nm laser excitation. (1: probe only; 2: 1mM glutathione (GSH); 3: 100 μ M homocysteine (Hcy); 4: 300 μ M cysteine (Cys); 5: 100 μ M H₂O₂; 6: 50 μ M HClO; 7: 50 μ M ONOO⁻; 8: 100 μ M NO; 9: 100 μ M Na₂S₄; 10: 100 μ M HSO₃²⁻; 11: 1 mM Ca²⁺; 12: 1 mM Zn²⁺; 13: 1 mM Mg²⁺; 14: 1 mM Fe²⁺; 15: 1 mM Cu²⁺; 16: 1 mM Ca²⁺; 17: 100 μ M NaHS; 18: 100 μ M NaHS + 300 μ M cysteine (Cys); 19: 100 μ M NaHS + 1mM glutathione (GSH); 20: 100 μ M NaHS + 100 μ M homocysteine (Hcy) (17-20, PBS/CH₃CN, 7:3, v/v, 20 mM, pH 6.2). (D) Photostability experiments of ICG, **WH-3** and **WH-3-HS** (WH-3 + 100 μ M NaHS) in PBS/CH₃CN mixture (7:3, v/v, 20 mM, pH 7.4) under continuous 808/980 nm excitation (200 mW/cm²) for 30 min with normalized fluorescent intensity.

24. Figure S11. Frontier orbitals of WH-X (WH-1, WH-2, WH-3, WH-4) obtained by DFT calculations.

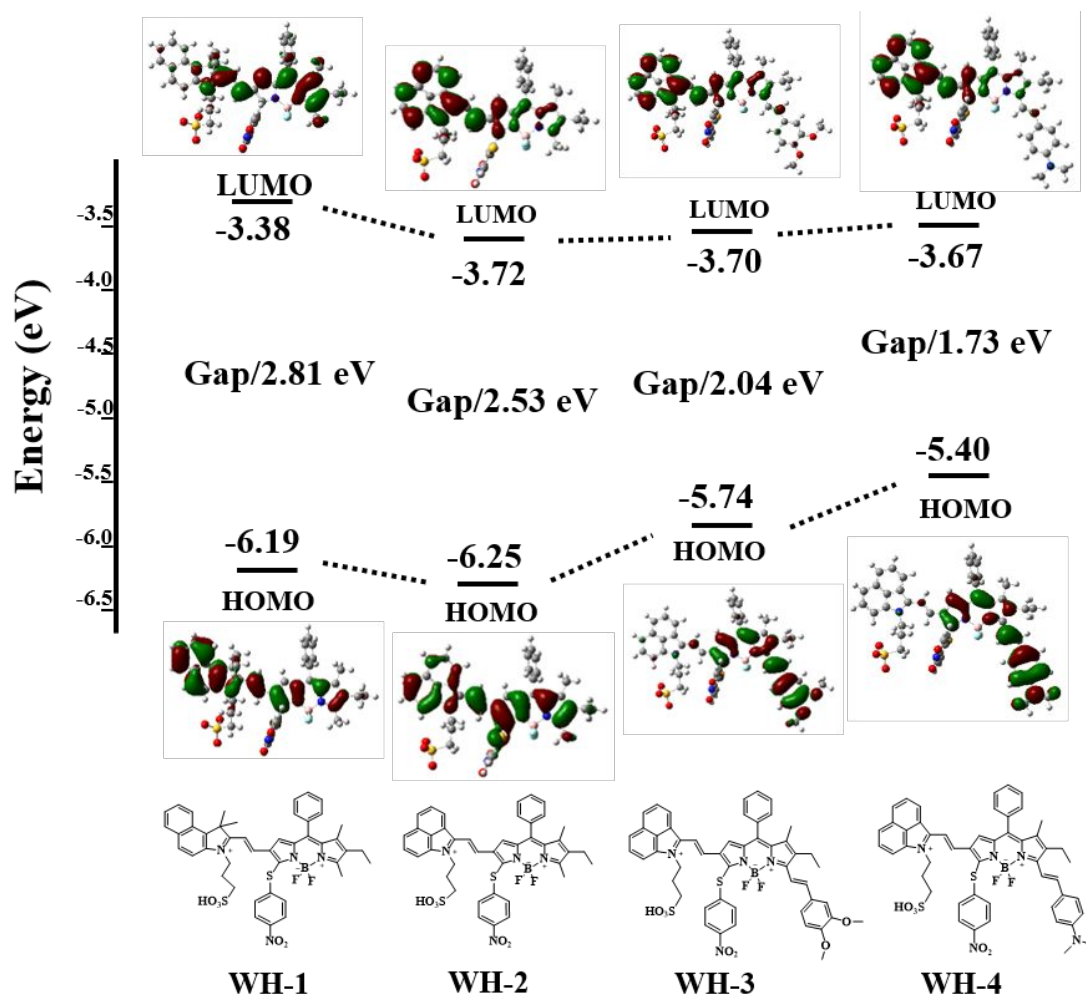


Figure S11. Frontier orbitals of WH-X (WH-1, WH-2, WH-3, WH-4) obtained by DFT calculations. The energy levels were computed at the same level of theory as WH-X-HS. Sulfonic groups were deprotonated under physiological pH.

25. Figure S12. High-resolution mass spectrometry confirmed reaction mechanism.

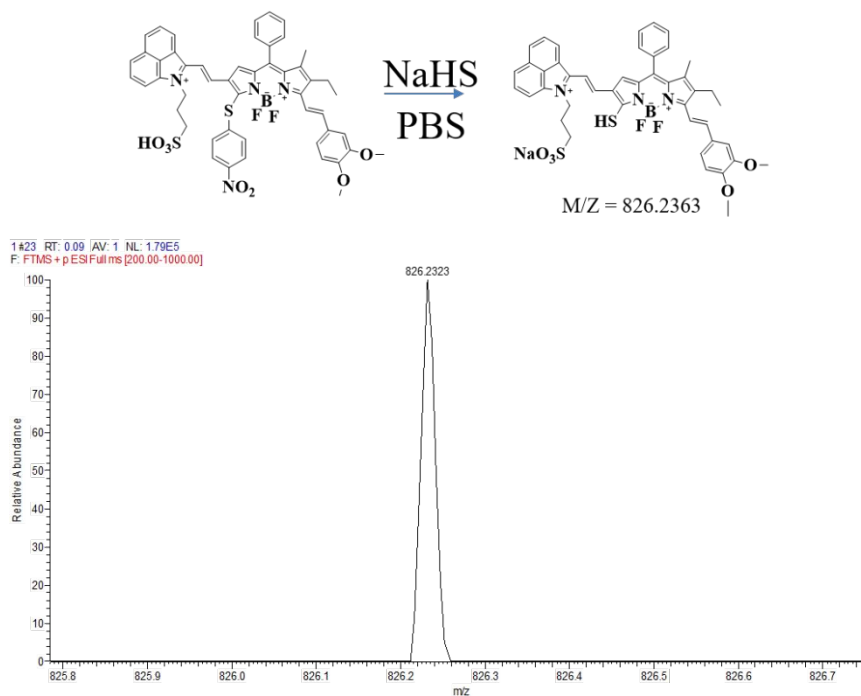


Figure S12. High-resolution mass spectrometry confirmed reaction mechanism.

26. Figure S13. Cytotoxicity of the WH-3.

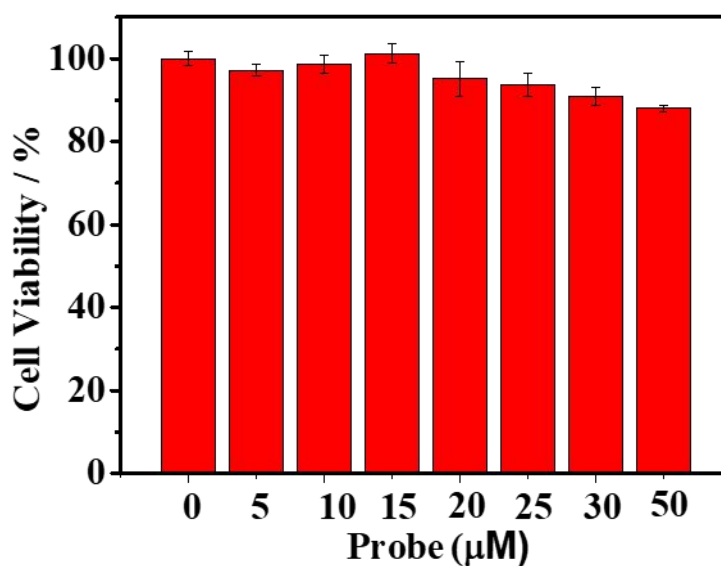


Figure S13. Cytotoxicity of the WH-3. Viability of HCT-116 cells incubated with different concentrations of WH-3 (0 μM, 5 μM, 10 μM, 15 μM, 20 μM, 25 μM 30 μM and 50 μM) for 24 hours.

27. Figure S14. H&E staining results of major organs.

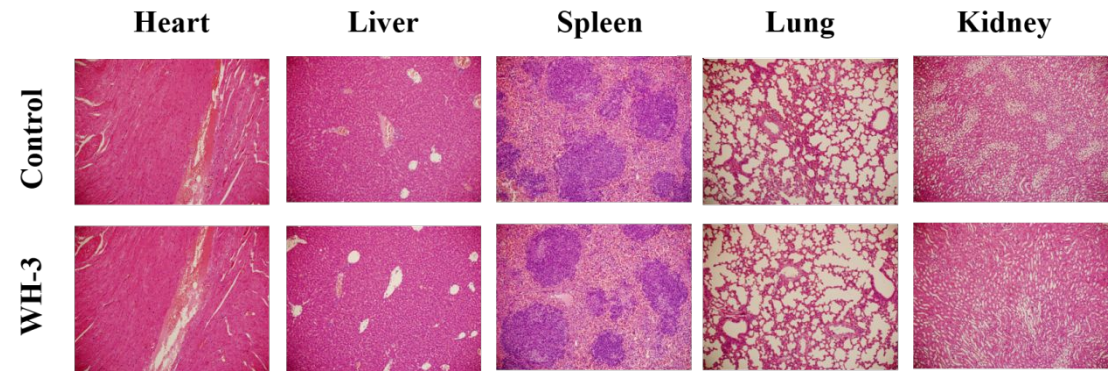
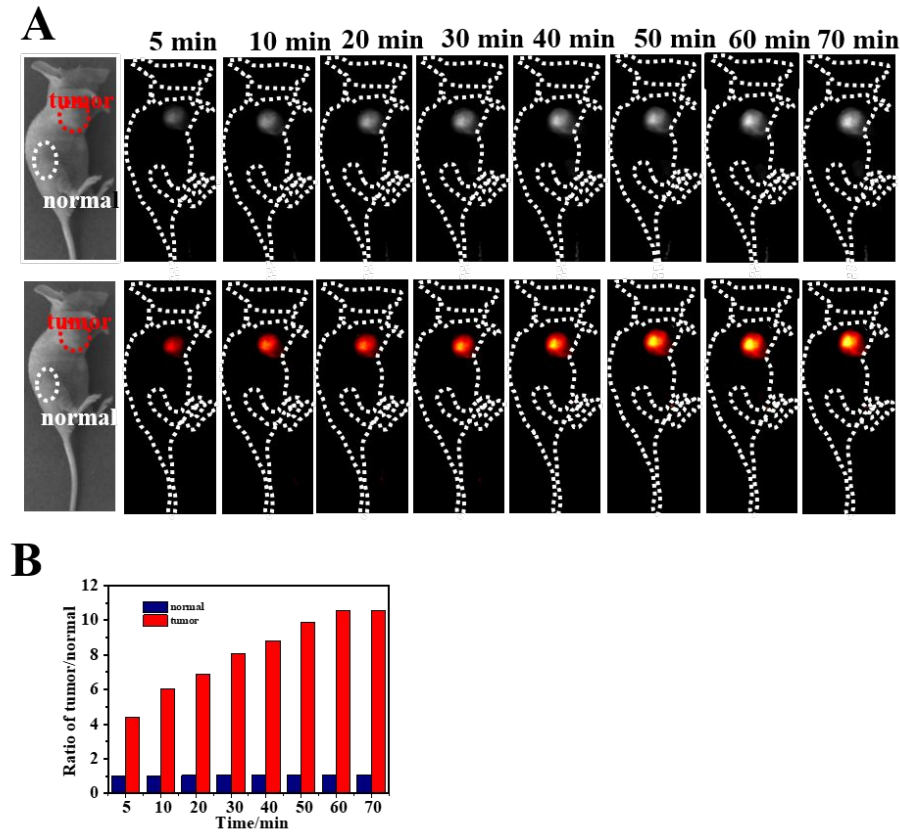


Figure S14. H&E staining results of major organs. H&E staining results of major organs (heart, spleen, liver, lung and kidney) collected from the control group and **WH-3** (100 μ L, 1.0 mM) treated group after 12 h post-injection. No obvious histological change in H&E staining was observed in those organs, suggesting **WH-3** has superior biocompatibility and biosafety.

28. Figure S15. In vivo imaging of H₂S in tumor-bearing mice.



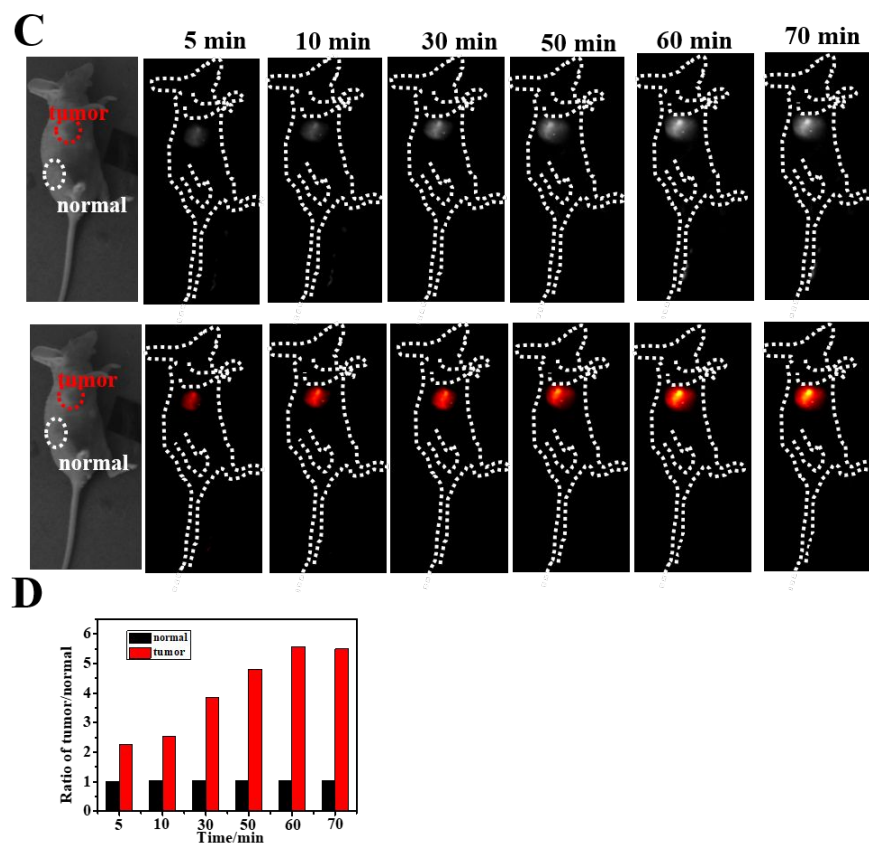


Figure S15. *In vivo* imaging of H₂S in tumor-bearing mice. The tumor regions and normal muscle of living mice were subcutaneously treated with **WH-3** and **WH-1** to verify the advantages of *in vivo* imaging of probes with long excitation and emission wavelengths. (A) *In vivo* NIR-II fluorescence imaging of **WH-3** (20 μ L, 1 mM) at different time points after orthotopic injection. (B) The fluorescence signal ratio between the tumor and normal muscle at various time points after the injection of **WH-3** according to region of interest measurements. Ex: 980 nm laser (80 mW/cm²), exposure time: 300 ms, 1100 nm LP. (C) *In vivo* NIR-II fluorescence imaging of **WH-1** (20 μ L, 1 mM) at different time points after orthotopic injection. (D) The fluorescence signal ratio between the tumor and normal muscle at various time points after the injection of **WH-1** according to average fluorescence intensity measurements. Ex: 808 nm laser (60 mW/cm²), exposure time: 300 ms, 1100 nm LP.

29. Figure S16. The advantage of long excitation and emission wavelength in penetration.

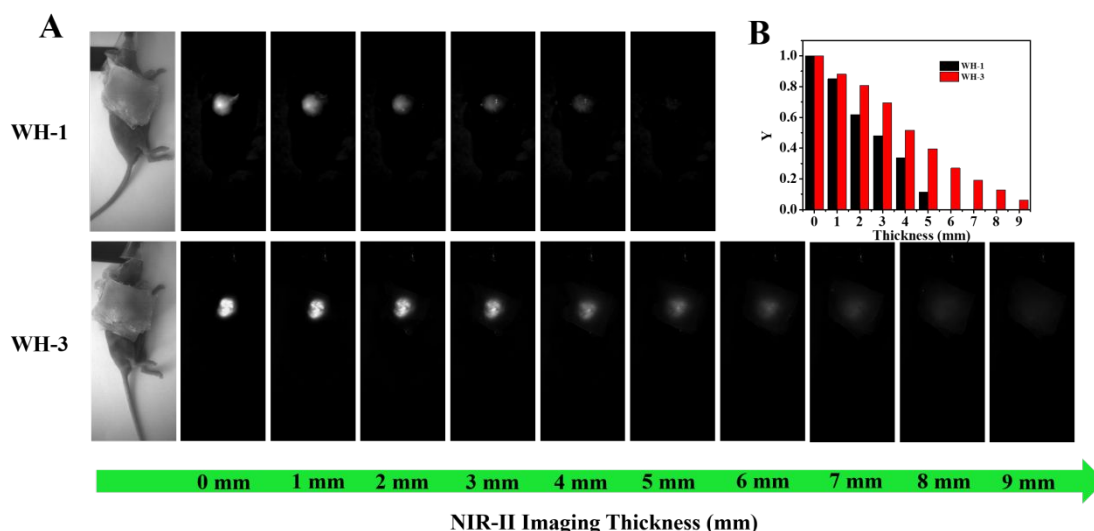


Figure S16. The advantage of long excitation and emission wavelength in tissue penetration. (A) NIR-II fluorescence penetration test of **WH-1** and **WH-3**. HCT-116 xenograft tumor-bearing mice were divided into two groups and orthotopic injected with **WH-3** and **WH-1** respectively. 60 min later, mice tumors were covered with varying thickness of pork tissue and subjected to *in vivo* imaging. **WH-3** (20 μ L, 1 mM) group, Ex: 980 nm laser (80 mW/cm²), exposure time: 300 ms, 1100 nm LP; **WH-1** (20 μ L, 1 mM) group, Ex: 808 nm laser (60 mW/cm²), exposure time: 300 ms, 1000 nm LP. (B) Fluorescence intensity changes as function of the thickness of pork tissues. The *ratio* Y was determined by fitting the fluorescence intensities of the samples according to the equation: $Y = (I_t - I_{black}) / (I_0 - I_{black})$. I_t represents the fluorescence intensity from samples covered by various thicknesses of pork tissues. I_{back} represents the fluorescence intensity of the background from pork tissue. I_0 represents the fluorescence intensity of the sample without covering pork tissue.

30. Figure S17. Time-dependent NIR-II imaging of endogenous H₂S changes by exogenous drug stimulation.

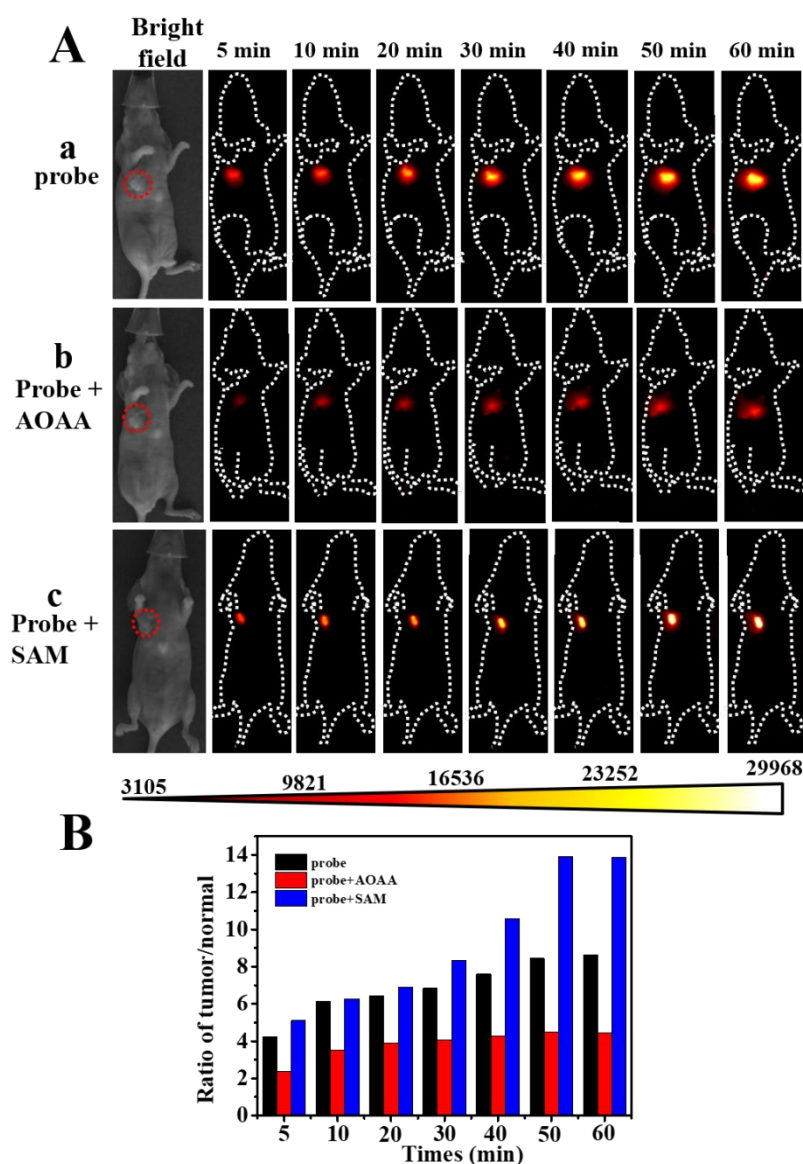
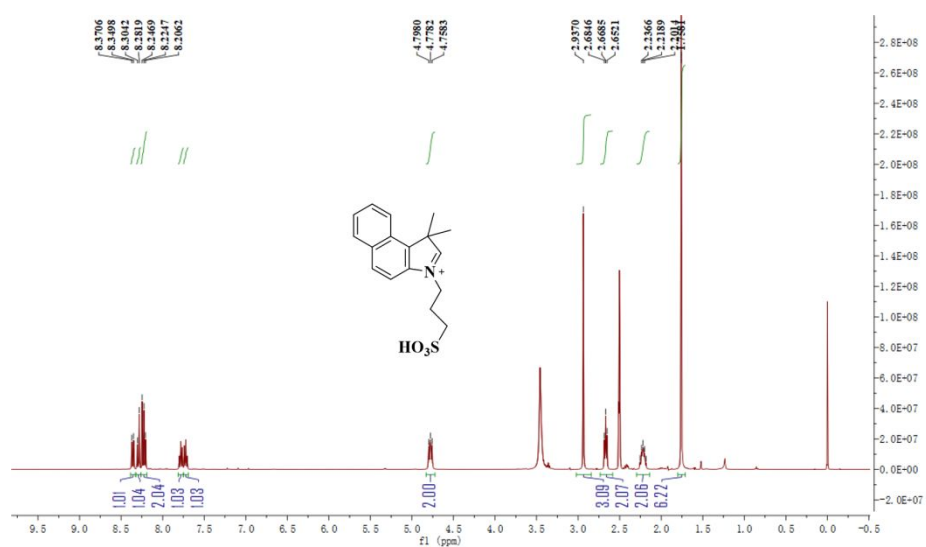
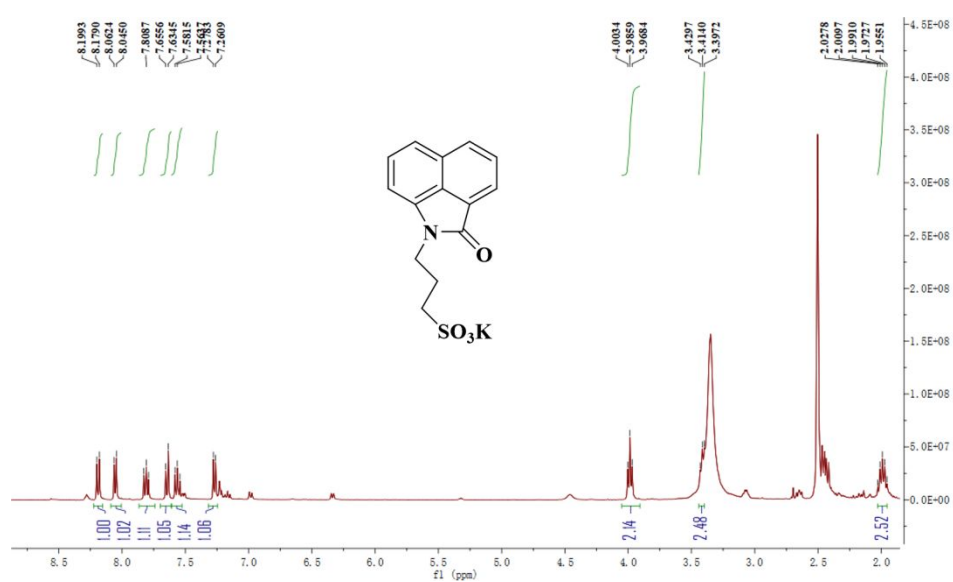


Figure S17. Time-dependent NIR-II imaging of endogenous H₂S changes by exogenous drug stimulation. (A-a) Mice only subcutaneous injected with **WH-3** (20 μ L, 1 mM). Time-dependent NIR-II imaging of mice were pretreated with (A-b) AOAA (25 μ L, 1 mM) and (A-c) SAM (25 μ L, 1 mM) for 6h, and then fluorescence images were collected at different time points after orthotopic injection of **WH-3** (20 μ L, 1 mM). (B) The fluorescence signal ratio between the tumor and normal muscle at various times after the injection of **WH-3** according to average fluorescence intensity measurements.

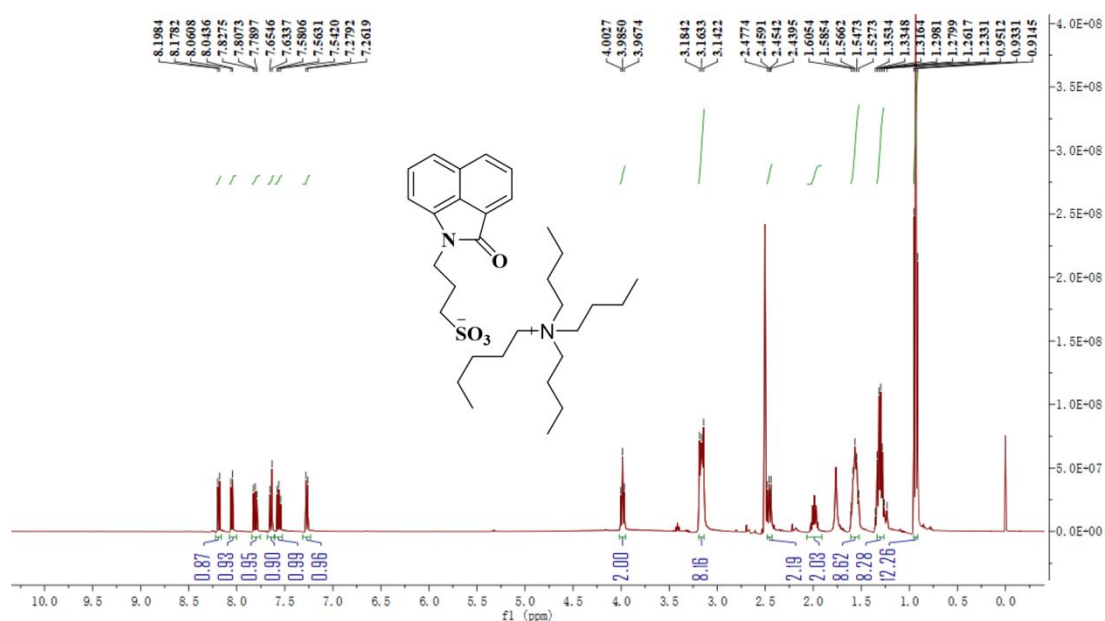
31. Figure S18. ^1H NMR of compound 1



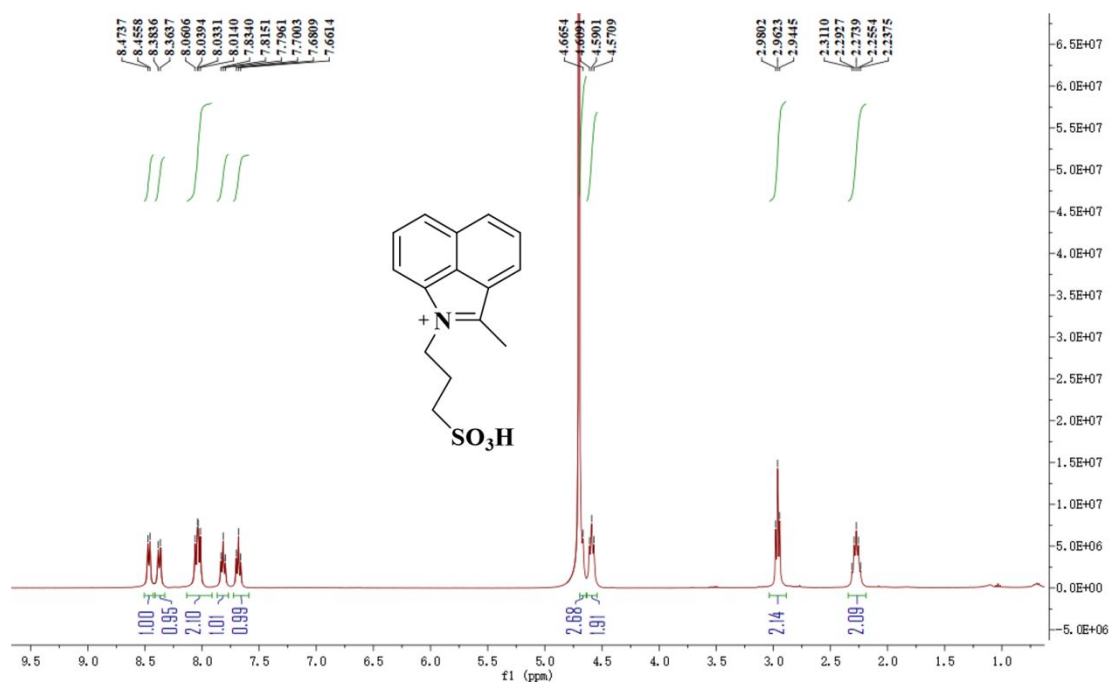
32. Figure S19. ^1H NMR of compound 2-1



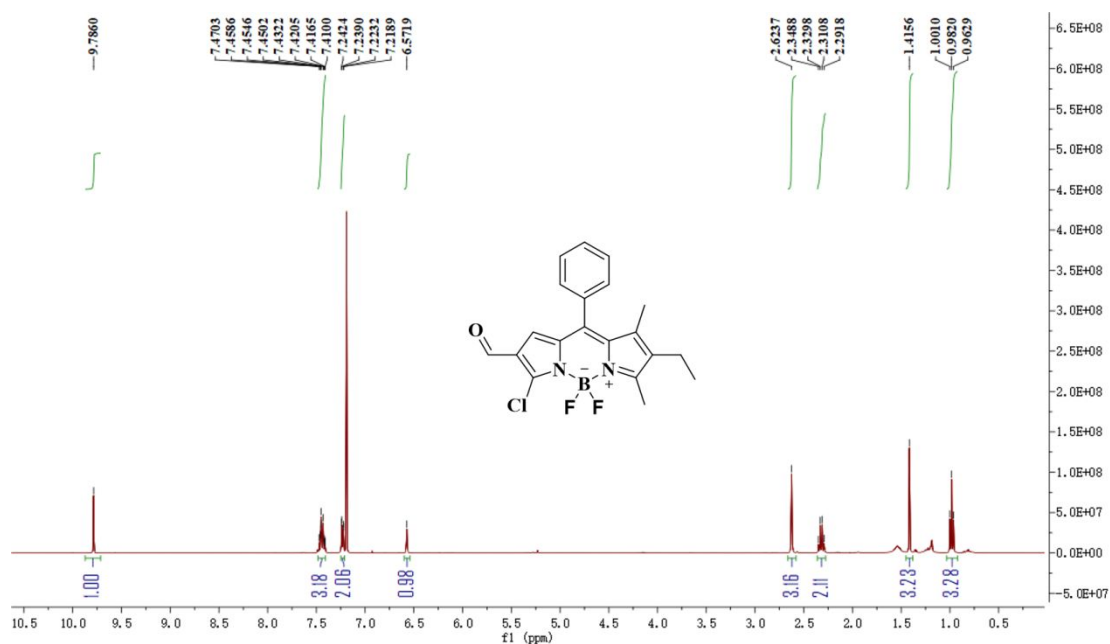
33. Figure S20. ¹H NMR of compound 2-2(1)



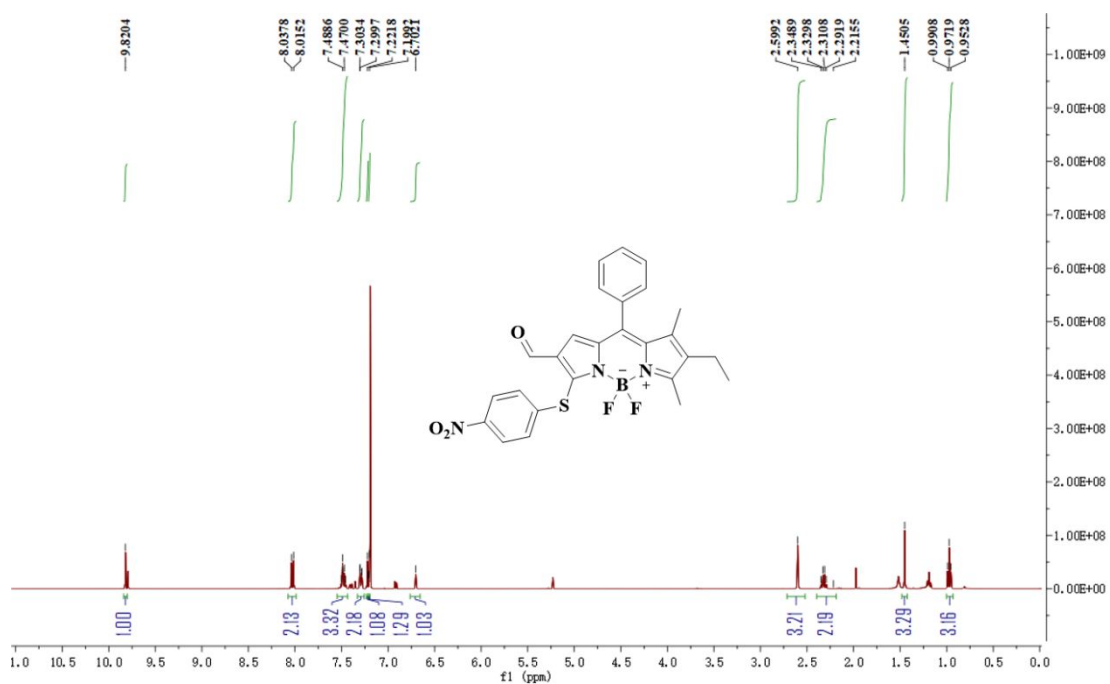
34. Figure S21. ¹H NMR of compound 2-2(2)



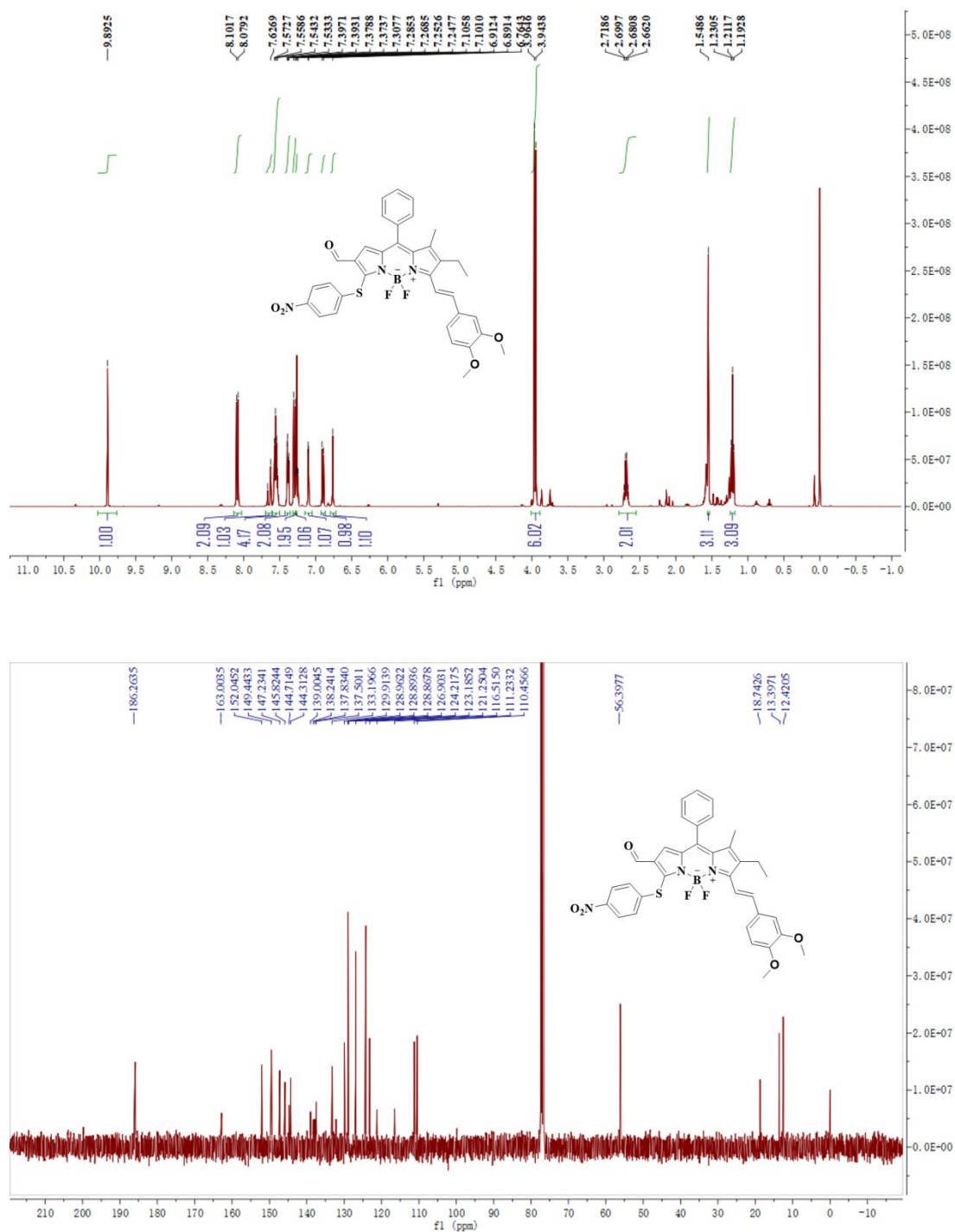
35. Figure S22. ^1H NMR of compound 3-1



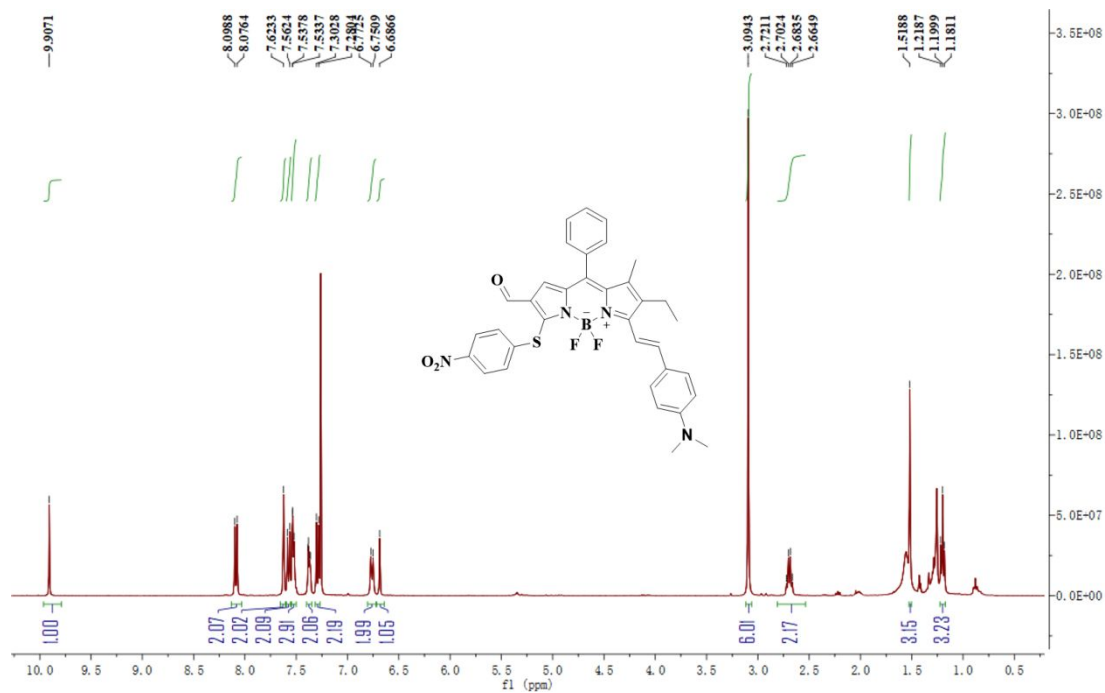
36. Figure S23. ^1H NMR of compound 3-2



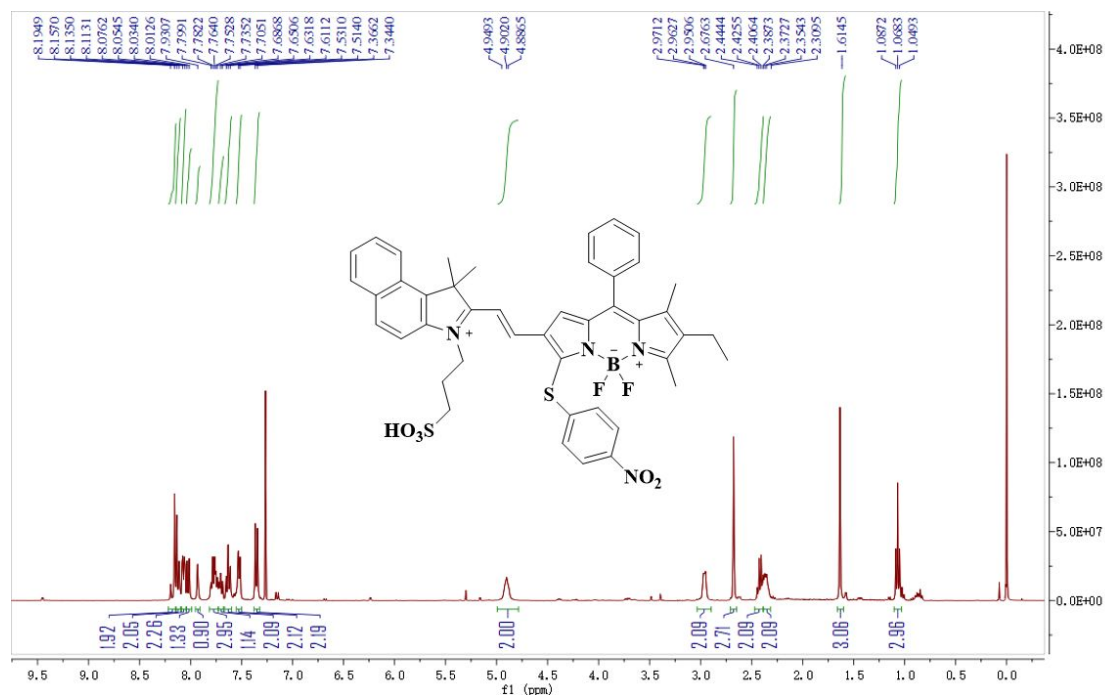
37. Figure S24. ^1H NMR and ^{13}C NMR of compound 3-3



38. Figure S25. ^1H NMR of compound 3-4



39. Figure S26. ^1H NMR and HRMS of probe WH-1



Chemical structure of compound 10 is shown above the mass spectrum. The structure is a complex boron-coordinated molecule featuring a phenyl group, a 4-nitrophenyl group, a 4-sulfamoylphenyl group, and a 1-methyl-4-(4-sulfamoylphenyl)-5H-indole-2-ylidene group.

Mass spectrum data (m/z vs. Relative Abundance):

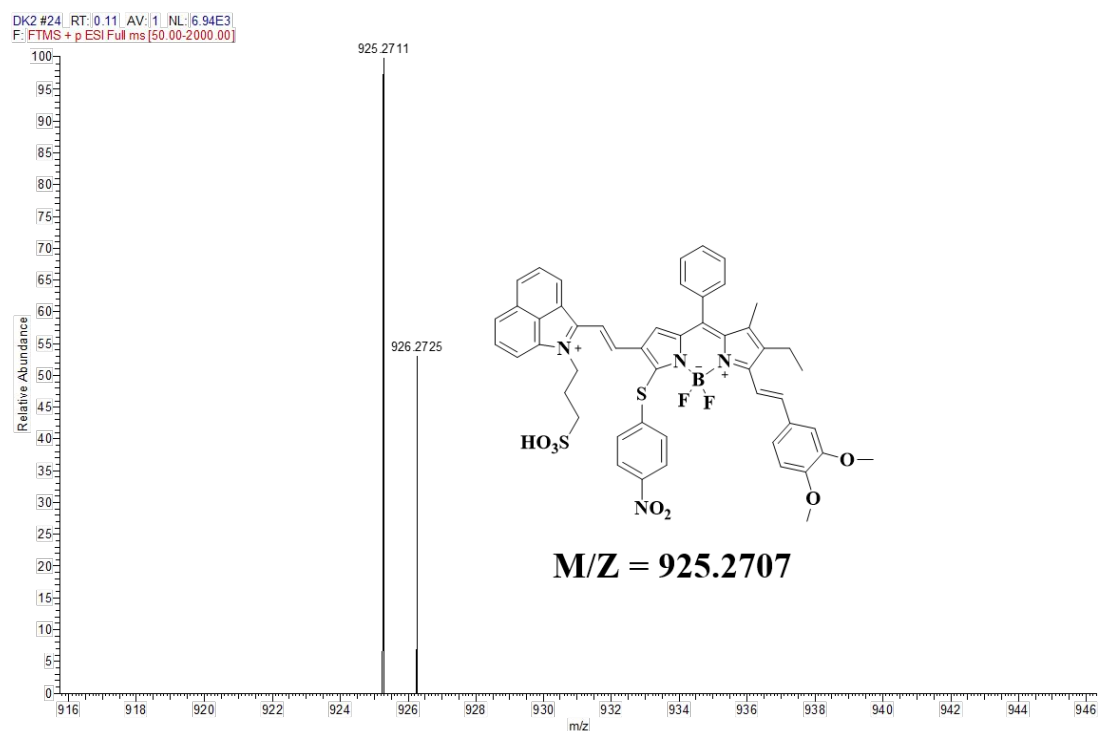
m/z	Relative Abundance (%)
610.1868	~1
649.4519	~1
666.1754	~1
688.1572	~1
719.2476	~1
742.3126	~1
764.2953	~1
791.2387	~1
813.2181	~5
819.2684	100
826.2227	~60
841.2487	~55
845.3025	~35
867.2856	~5
899.2093	~5

Chemical Structure of Compound 10:

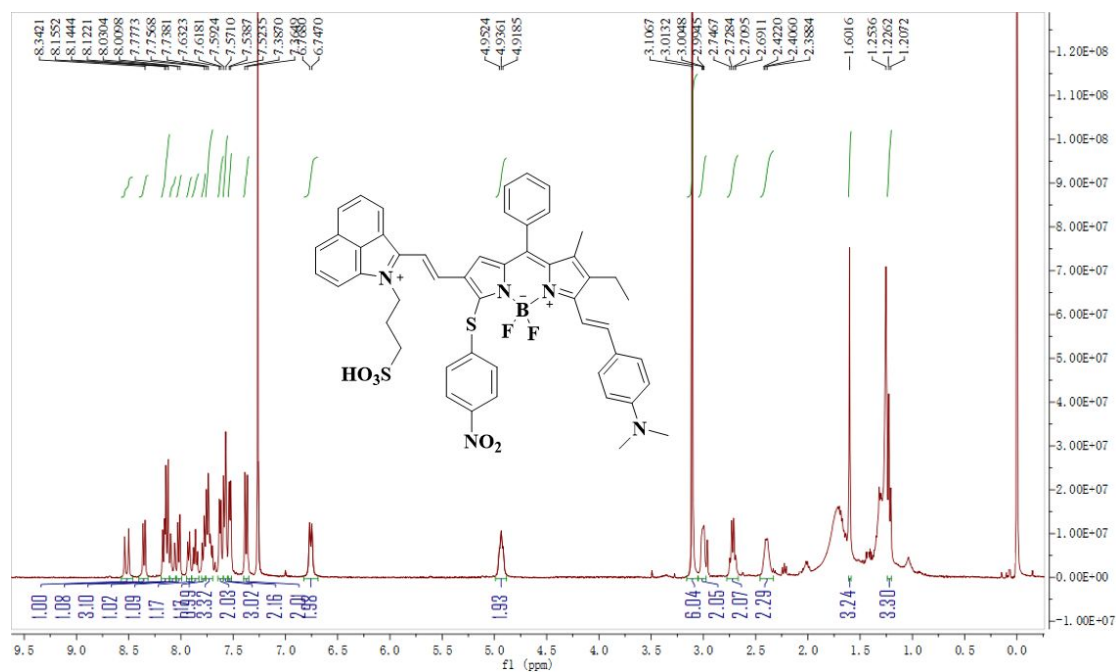
CC1=C(C)N(C2=CC=CC=C2)B(F)(F)N2C=C(C3=CC=CC=C3)C4=CC=CC=C4N4CCCC4S(=O)(=O)O

¹H NMR Spectrum (DMSO-d₆):

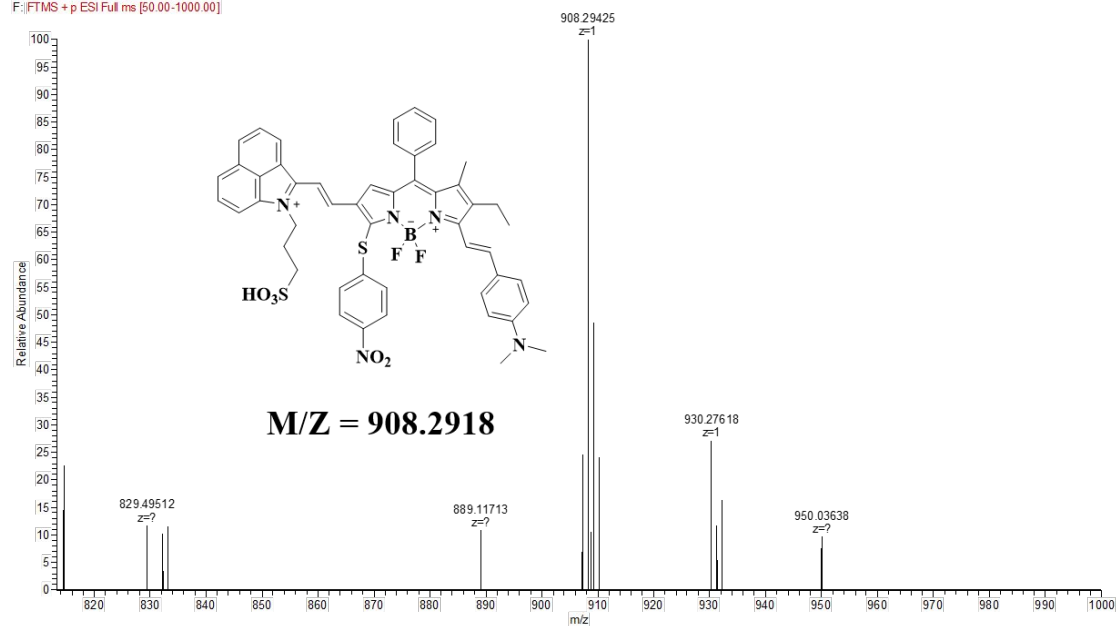
Chemical Shift (ppm)	Integration
8.4039, 8.4352, 8.3853, 8.3652, 8.2906, 8.2519, 8.1718, 8.1528, 8.1442, 8.1218, 8.0547, 8.0342, 7.9154, 7.8951, 7.8740, 7.8547, 7.8259, 7.8070, 7.7854, 7.7774, 7.7592, 7.7407, 7.7319, 7.5416, 7.5244, 7.3699, 7.3477	1.00, 1.03, 3.03, 3.03, 1.05, 2.02, 2.02, 4.05, 2.02, 2.02
4.9818, 4.9636, 4.9447	2.00
2.9976, 2.9913, 2.9800, 2.6748, 2.4462, 2.4273, 2.4082, 2.3895	2.00, 3.10, 4.05
1.6116	3.14
1.0884, 1.0696, 1.0596	3.03



42. Figure S29. ^1H NMR and HRMS of probe WH-4



DK1#25 RT:0.10 AV:1 NL:4.51E4
F:FTMS+p ESI Full ms [50.00-1000.00]



43. References

- [1] Tao, Z.; Hong, G.; Shinji, C.; Chen, C.; Diao, S.; Antaris, A. L.; Zhang, B.; Zou, Y.; Dai, H. Biological Imaging Using Nanoparticles of Small Organic Molecules with Fluorescence Emission at Wavelengths Longer than 1000 nm. *Angew. Chem. Inter. Ed.* **2013**, *52*, 13002-13006.
- [2] Chen, J. A.; Pan, H.; Wang, Z.; Gao, J.; Tan, J.; Ouyang, Z.; Guo, W.; Gu, X. Imaging of ovarian cancers using enzyme activatable probes with second near-infrared window emission. *Chem. Commun.* **2020**, *56*, 2731-2734.
- [3] Wang, R.; Chen, J.; Gao, J.; Chen, J. A.; Xu, G.; Zhu, T.; Gu, X.; Guo, Z.; Zhu, W. H.; Zhao, C. A molecular design strategy toward enzyme-activated probes with near-infrared I and II fluorescence for targeted cancer imaging. *Chem. Sci.* **2019**, *10*, 7222-7227.
- [4] Ren, T. B.; Wang, Z. Y.; Xiang, Z.; Lu, P.; Lai, H. H.; Yuan, L.; Zhang, X. B.; Tan, W. A General Strategy for Development of Activatable NIR-II Fluorescent Probes for in vivo High-Contrast Bioimaging. *Angew. Chem. Int. Ed.* **2021**, *60*, 800-805.
- [5] Ouyang, J.; Sun, L.; Zeng, Z.; Zeng, C.; Zeng, F.; Wu, S. Nanoaggregate Probe for Breast Cancer Metastasis through Multispectral Optoacoustic Tomography and Aggregation-Induced NIR-I/II Fluorescence Imaging. *Angew. Chem. Int. Ed.* **2019**, *59*, 10111-10121.
- [6] Li, D.; Wang, S.; Lei, Z.; Sun, C.; El-Toni, A. M.; Alhoshan, M. S.; Fan, Y.; Zhang, F. Peroxynitrite Activatable NIR-II Fluorescent Molecular Probe for Drug-Induced Hepatotoxicity Monitoring. *Anal. Chem.* **2019**, *91*, 4771-4779.
- [7] Meng, X.; Zhang, J.; Sun, Z.; Zhou, L.; Deng, G.; Li, S.; Li, W.; Gong, P.; Cai, L. Hypoxia-triggered single molecule probe for high-contrast NIR II/PA tumor imaging and robust photothermal therapy. *Theranostics* **2018**, *8*, 6025-6034.
- [8] Feng, W.; Zhang, Y.; Li, Z.; Zhai, S.; Lv, W.; Liu, Z. Lighting Up NIR-II Fluorescence in Vivo: An Activable Probe for Noninvasive Hydroxyl Radical Imaging. *Anal. Chem.* **2019**, *91*, 15757-15762.
- [9] Dale, T. J.; Rebek J. Fluorescent Sensors for Organophosphorus Nerve Agent Mimics. *J. Am. Chem. Soc.* **2006**, *128*, 4500-4501.